Culture on graphene composite scaffolds enhances function of stem cell derived cardiomyocytes

Pamela Hitscherich (1), Ashish Aphale (2), Richard Gordan (3), Lai-Hua Xie (3), Prabir Patra (2,4), Eun Jung Lee (1)

(1) New Jersey Institute of Technology, Department of Biomedical Engineering
(2) University of Bridgeport, Department of Biomedical Engineering
(3) Rutgers New Jersey Medical School, Department of Cell Biology and Molecular Medicine
(4) University of Bridgeport, Department of Mechanical Engineering

Contractile behavior of the heart relies on directed signal propagation through the electroconductive networks that exist within the native myocardium. Electroactive scaffolds, such as carbon-based nanostructured scaffolds, have emerged as promising candidate materials for cardiac tissue engineering applications due to their unique properties. In this work, the biocompatibility and feasibility of a novel three-dimensional (3D) graphene-embedded poly(caprolactone) (PCL+G) nanocomposite scaffold were examined using mouse stem cell-derived cardiomyocytes (mES-CM). High magnification SEM allowed for visualization of graphene particles embedded within the PCL matrix of out 15% PCL+G scaffolds (A). XRD analysis also confirmed the presence of graphene within PCL+G scaffolds samples (B). Results demonstrated that mES-CM adhere well and strongly express cardiac specific gene marker, cardiac troponin T when cultured on PCL+G scaffolds (C). MES-CM also had high cell viability (D) and aligned along the major fiber axis with well-registered sarcomeres (E), exhibiting phenotypic characteristics of native cardiomyocytes. Moreover, the presence of graphene providing local conductive networks within the 3D scaffolds promoted functional improvements and maturity of stem cell-derived cardiomyocytes as PCL+G scaffolds facilitated functional Ca^{2+} handling behavior of mES-CM. Specifically, mES-CM responded to challenges with 10 mM caffeine (F), contract spontaneously at the highest frequency (G) and promoted enhanced fractional Ca^{2+} release (H) and caffeine induced transient T_{50} (I). Thus, the presence of graphene within the 3D scaffolds promoted functional improvements in calcium handling and maturity of stem cell-derived cardiomyocytes.

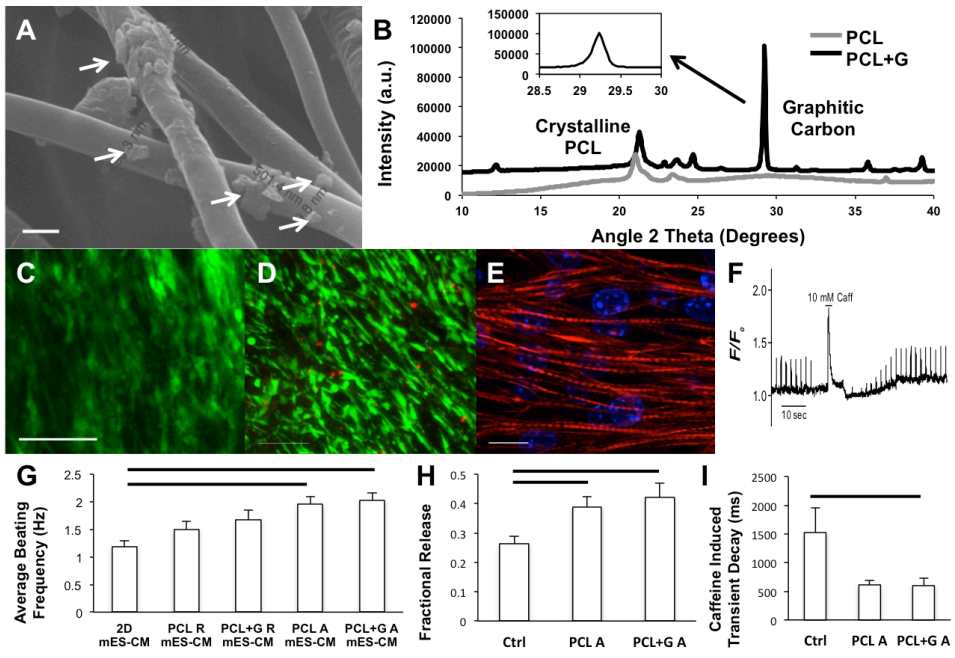

Composite-mediated Angiogenesis to Enhance the Survival of Transplanted Human Adipose Stem Cells

Brian H. Cho(1, 2,),[†] Xiaowei Li(2, 3, 4),[†] Sashank Reddy(1), Russell Martin(2, 3, 4), Michelle Seu(1, 2), Gurjot Walia(1), Justin M. Sacks(1)[*], Hai-Quan Mao(2, 3, 4,)[*]

1. Department of Plastic and Reconstructive Surgery, 2. Translational Tissue Engineering Center, 3. Department of Materials Science & Engineering, and 4. Institute for NanoBioTechnology, Johns Hopkins University, Baltimore, MD 21218, USA

[†]These authors contributed equally to this work. [*]Corresponding authors

Introduction: Devastating soft tissue losses from tumor extirpation, trauma, aging, or congenital malformation affect millions of people each year. Existing options for soft tissue restoration have significant drawbacks: using autologous tissue flaps causes donor-site defects; prosthetic implants are prone to foreign-body response leading to fibrosis; and fat grafting and dermal fillers are limited to small volume defects and only provide transient volume restoration.[1] Human adipose-derived stem cells (hASCs) are easily isolated for autologous transplantation, making them promising for clinical application. Transplantation of isolated hASCs, however, has several key hurdles, such as low cell survival rate, poor cell retention, and lack control of cell differentiation. To address these hurdles, we have developed a unique nanofiber-hydrogel composite with interfacial bonding, which allows independent tuning of bulk mechanical properties and porosity of the hydrogel phase, enabling both cell infiltration and structural integrity. We hypothesize that our unique nanofiber-hydrogel composite will aid host vascular ingrowth to support the survival of transplanted hASCs and also assist the migration of hASCs for soft tissue regeneration.

Materials and Methods: To prepare the composite, we functionalized polycaprolactone (PCL) fibers with maleimide groups and conjugated to thiol-modified hyaluronic acid (HA) hydrogel matrix through Michael-type addition chemistry. We used a rheometer to characterize the mechanical properties of our composites. We subcutaneously injected the composite with hASC spheroids and assessed the angiogenesis, transplanted cell survival and differentiation by immunohistochemistry.

Results and Discussion:

Mechanically tunable composite to promote cell migration and vascularization *in vitro*. To mimic native soft tissue, we have developed a nanofiber-composite with similar ultrastructure and porosity (Data not shown). We modulated our composite to have similar mechanical properties to fresh fat tissue [Storage modulus (G') = 150 Pa], while the hydrogel phase in our composite maintains high porosity (80 Pa). We fabricated hASC spheroids of uniformed size (200 μm in diameter) and seeded them inside soft hydrogel (80 Pa), medium hydrogel (150 Pa), and composite (150 Pa). Human ASCs within the composite migrated the longest distance among all three groups at day 14 (**Fig. 1 a-b**; 203 *vs.* 122, and 0 μm; $P<0.05$). To optimize our composite for vascularization, we adopted an established *in vitro* vascularization model.[2] The cells in our composite spontaneously initiated vascular morphogenesis to form multicellular tubular structures with branching and visible open luminal spaces starting as early as 2 days in culture, which was not seen in the medium hydrogel. At day 7, the cells formed 3D tubular networks with increased interconnection and highest network density within our composite (**Fig. 1c-d**, 16.4 *vs.* 12.4, and 2.1 mm/mm^2; $P<0.05$).

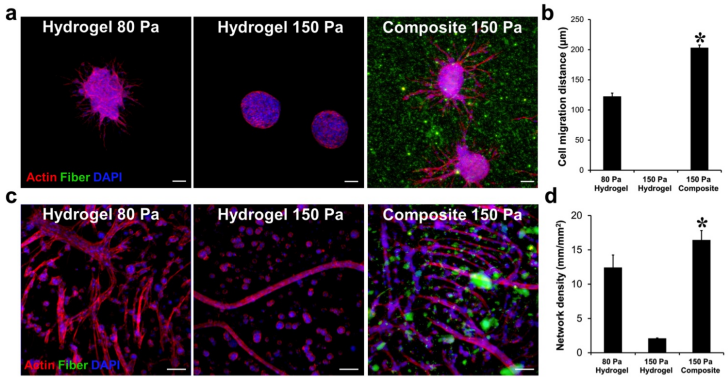

Figure 1. (**a-b**) Human ASCs migrated the longest distance in the composite. (**c-d**) Vascular network with the highest density was observed in our composite. Fibers were loaded with F8BT in green. Cell nuclei were stained with DAPI in blue. Cell morphology was stained with Phalloidin 568 in red. Scale bar: 100 μm

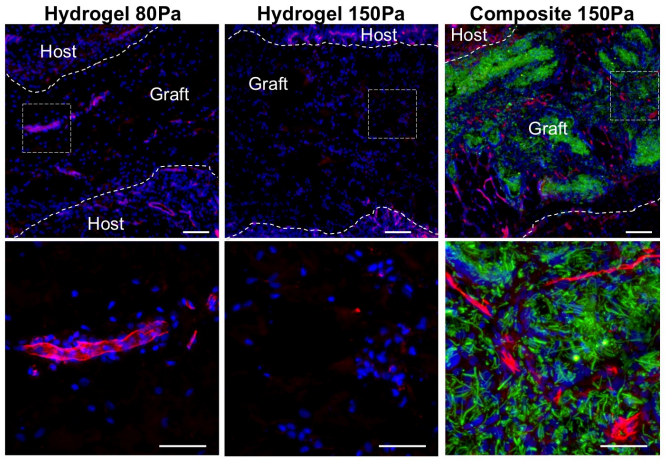

Figure 2. Composite induced host blood vessel ingrowth. Host blood vessels were stained with RECA-1 in red. Fibers were loaded with F8BT in green. Cell nuclei were stained with DAPI in blue. Scale bar: 100 μm.

Composite-mediated angiogenesis to enhance the survival of transplanted hASCs *in vivo*. To investigate the biocompatibility of our composite and its ability to promote hASC survival and differentiation, we subcutaneously injected hASC spheroids with the composite and hydrogels into the backs of Lewis Rats. After transplantation, animals exhibited no signs of infection or inflammation. At post-operative day (POD) 7, the highest density of host blood vessels were identified in the composite group (**Fig. 2**). Transplanted hASCs showed a higher degree of survival and spreading within our nanofiber-hydrogel composite compared to those in the hydrogels (**Fig. 3).** Host blood vessels followed the nanofibers within the composite to support transplanted cells. Improved cell survival was also observed within our composite at POD 28. We currently are investigating the differentiation of transplanted hASCs mediated by our composite.

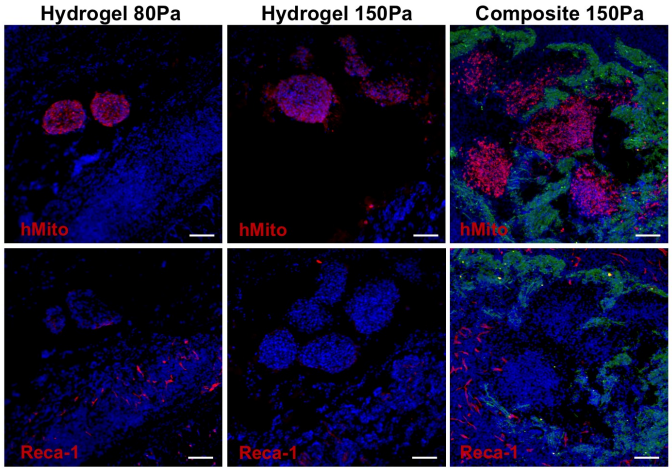

Figure 3. Transplanted hASCs (human mitochondria+, red, top panel) within our composite were supported by host blood vessels (RECA-1+, red, bottom panel) at POD 7. Fibers were loaded with F8BT in green. Cell nuclei were stained with DAPI in blue. Scale bar: 100 μm.

Conclusion: We optimized a mechanically tunable nanofiber-hydrogel composite that mimics the structure and mechanical property of adipose tissue. The optimized composite promoted host vascular ingrowth and supported the survival of transplanted hASCs.

References: 1. Banyard DA et. al. *J Cell Mol Med*, 2015, 19(1): 21-30. **2**. Hutton DL et. al. *Tissue Eng Part A*, 2016, 22(1-2): 161-169.

Differentiation of Anterior Foregut Endoderm and Maintenance of Phenotype when Seeded in a Decellularised Rat Lung

Adam Mitchell[1], Charles Drinnan[1], Todd Jensen[1], Christine Finck[1,2]

[a] Department of Pediatrics, University of Connecticut Health Center, Farmington, CT, USA
[b] Department of Surgery, Connecticut Children's Medical Center, Hartford, CT, USA

There is a growing trend of utilising decellularised lung matrices as scaffolds for lung regeneration and disease modelling. Ideally, these scaffolds would be seeded with patient-specific induced pluripotent stem cells (iPSCs), but current differentiation protocols are not optimal. Many protocols are available for the directed differentiation of iPSCs to a desired cell phenotype such as hepatic, pancreatic and pulmonary cells. In order to produce cells with an alveolar-like phenotype iPSCs are first differentiated through definitive endoderm (DE) and anterior foregut endoderm (AFE) intermediaries. The production of alveolar like cells in this manner is both time consuming (25+ days) and expensive, whereas, the production of AFE is relatively cheap and expedient (5 days). The aim of this study was the production of AFE cells and demonstrating their engraftment into decellularised rat lungs.

iPSCs were differentiated first to DE using CHIR99021 for 1 day and activin A for 3 days and assessed by flow cytometry for CXCR4 and EpCAM expression. AFE was induced by treatment with dorsomorphin/SB431542 and IWR1/SB431542 each for 1 day and assessed by flow cytometry, immunofluorescence and qRT-PCR for FOXA2 expression. Rat heart/lung blocks were removed and placed on to a bioreactor system. SDS was perfused through the vasculature under a constant pressure of 30 cm H_2O for 2 hours then rinsed overnight in DI water. The following day 30 million AFE cells were gravity fed into the lungs through the trachea and allowed to culture for 3 days. Cell engraftment and phenotype was assessed with histology.

After 3 days of DE induction cells tested >95% $CXCR4^+EpCAM^+$ by flow cytometry. Following a further two days of AFE induction, dissociation in Tryple and replating (to remove undifferentiated cells), samples tested >97% $FOXA2^+$ with expression confirmed by immunofluorescence and qRT-PCR. Upon three days of culture inside decellularised rat lungs there was a near uniform distribution of AFE cells throughout the scaffold and the expression of FOXA2 was maintained. Finally, upon closer examination AFE cells had begun to align with the matrix in the scaffold and form the beginnings of a continuous barrier in the larger airways and blood vessels.

AFE cells can be differentiated sooner and at a lower cost than terminally differentiated lung cells. Our data demonstrate that AFE cells can engraft into a decellularised lung scaffold without losing their phenotype. Future studies will assess whether the scaffold itself is sufficient to direct the differentiation of these cells to a pulmonary fate.

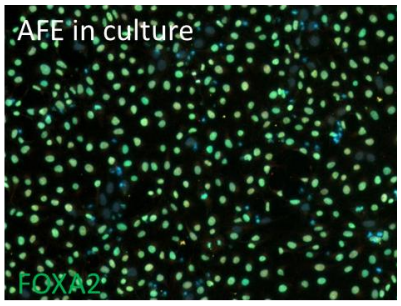

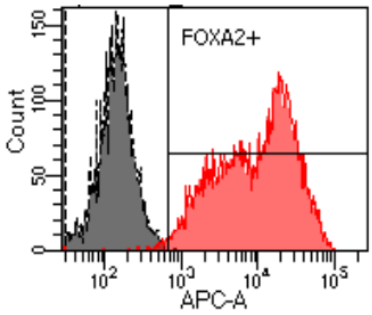

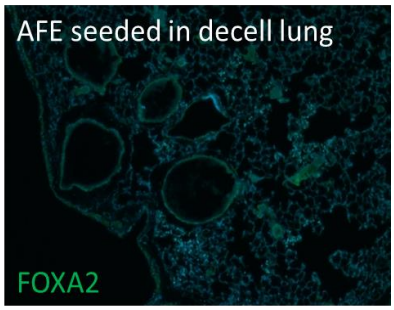

Dipyridamole-Coated 3D-Printed Bioactive Ceramic (3DPBC) Scaffolds in Sheep Calvaria to Grow New Bone

Leyla Cavdar(1), Jonathan Bekisz(2), Christopher Lopez(3), Roberto Flores(2), Andrew Torroni(2), Lukasz Witek(1), Bruce Cronstein(4), Paulo Coelho(1, 2)

1. Department of Biomaterials and Biomimetics, New York University College of Dentistry, New York, NY, USA
2. Hansjörg Wyss Department of Plastic Surgery, New York University School of Medicine, New York, NY, USA
3. Icahn School of Medicine at Mount Sinai, New York, NY, USA
4. Department of Medicine, New York University Langone Medical Center, New York, NY, USA

Statement of Purpose: Creating healthy bone is necessitated by bone defects that arise from trauma, tumor resection, or congenital lesions, and such defects must be adequately addressed since bone provides homeostatic and biomechanical functions [1, 2]. For example, in treating skull deformities in patients with craniosynostosis, calvarial reconstruction helps restore skull shape and protect intracranial matter [3]. However, this approach may result in structural abnormalities due to inevitable spatial gaps left over between skull fragments. Additionally, calvarial reconstruction can be challenging when a resected cancerous lesion is too deep or large for restoration [4]. Given current practice shortcomings, tissue engineering offers considerable promise in regrowing new bone. For instance, scaffolds provide a structure for three-dimensional tissue development, and also harbor osteoconductive properties to promote bone growth. To further elucidate the role of such scaffolds, this research examines the efficacy of dural-mediated bone growth upon implantation of dipyridamole-coated 3D-printed bioactive ceramic (3DPBC) scaffolds (inlays) into calvarial defects using the sheep model.

Methods: 3DPBC scaffolds that were porous to the dura mater were custom-designed and printed, and either coated in only collagen (control) or coated in collagen and then immersed in 100 µM dipyridamole (experimental). Sheep (N=5) were subjected to calvarial defects (with 11 mm diameter) via two separate operations, and the scaffolds were implanted anteriorly (control) and posteriorly (experimental) on the left side (6 weeks) and right side (3 weeks) of the calvaria. After the sheep were euthanized and the histological samples were processed, three regions of interests were selected: scaffold including cap, core of scaffold not including cap, and 50% of interior width of scaffold (figure 1). The defects were analyzed through histomorphometry and microcomputed tomography in order to quantify the bone, scaffold, and soft tissue as a function of time and distance. Statistical analysis was performed to determine the significance of results using a 95% confidence interval.

Results: There were no signs of inflammation or ectopic bone formation within the defects. Analyses demonstrated that the 3DPBC scaffolds treated with dipyridamole exhibited significantly improved bone growth (more than 60%) in the regions of interest when compared to scaffolds treated only with collagen ($p<0.04$). Furthermore, a significantly higher percentage of bone formation was evident in the defects that were left for 6 weeks when compared to 3 weeks ($p<0.01$). It should be noted that this increase in bone percentage with respect to time appears to be independent of scaffold group. When examining bone as a function of distance, bone growth percentage greatly decreased as it furthered away from the edge of the calvarial defect.

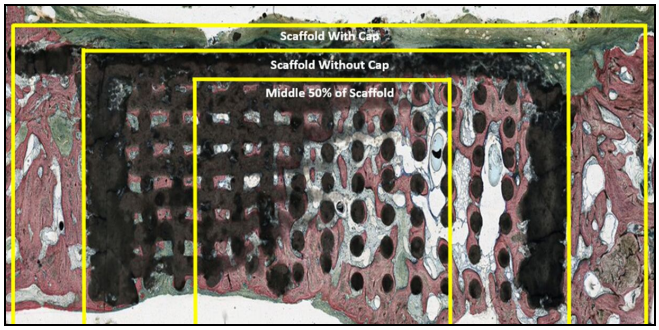

Figure 1: Histologic image depicting three regions of interest used for tissue composition analysis

Conclusion: 3DPBC scaffolds that were treated with the bone forming agent dipyridamole and/or left longer in the bone defect demonstrate considerably higher bone percentage and thus improved osteogenesis *in vivo* within the calvarial defect of sheep.

References:

1. Beasley NJ, Gilbert RW, Gullane PJ, Brown DH, Irish JC, Neligan PC (2004). Scalp and forehead reconstruction using free revascularized tissue transfer. Arch Facial Plast Surg 6(1):16–20
2. Clarke B (2008). Normal bone anatomy and physiology. Clin J Am Soc Nephrol 3: S131–S139
3. Lin S, Hanasono MM, Skoracki RJ (2008). Scalp and Calvarial Reconstruction. Seminars in Plastic Surgery 22(4): 281-293
4. Stark J, Podda S, & Szymanski K (2016). Invasive Squamous Cell Carcinoma of the Scalp and Calvarium: A Multidisciplinary Approach. Eplasty 16, e29

3D-Printed Beta-Tricalcium Phosphate Scaffolds for the Treatment of Alveolar Cleft Defects: A Pilot Study in Rabbits

Fady Gendy[1], Jonathan Bekisz[2], Christopher Lopez[1,3], Roberto Flores[4], Andrew Torroni[4], Lukasz Witek[1], Paulo Coelho[1,4]

[1]Department of Biomaterials and Biomimetics, New York University College of Dentistry, New York, NY, USA, [2]New York University School of Medicine, New York, NY, USA,[3]Icahn School of Medicine at Mount Sinai, New York, NY, USA, [4]Hansjörg Wyss Department of Plastic Surgery, New York University Langone Medical Center, New York, NY, USA

Purpose: Clefts of the lip or palate are a common craniofacial anomaly which affects approximately 1 in every 700 births worldwide [1]. Insufficient bony stock of the maxilla, resulting in an alveolar cleft, is a highly prevalent secondary complication in patients born with a cleft palate. Autologous bone grafts are the current standard of reconstruction, but are limited due to the amount of bone that can be retrieved. Autologous bone grafts also present danger of pain, fracture or infection at the donor site along with high risks of failure [2]. Research efforts have turned to bone tissue engineering for a potential biomaterial-based solution capable of generating osseous tissue in the alveolar cleft. Recent studies have demonstrated the potential clinical and therapeutic applications of beta-tricalcium phosphate (β-TCP). While this biomaterial is a known component of vertebrate bone with well-established osteogenic properties, its capacity for adaptation to any size or shape through 3D-printing optimizes its ability to generate osseous tissue. This study utilizes a rabbit model to investigate the suitability of 3D-printed β-TCP scaffolds for the reconstruction of an alveolar cleft defect, a common abnormality in patients with congenital cleft palates.

Methods: A cohort of five skeletally-mature New Zealand White rabbits underwent a surgical procedure in which a unilateral, ~4.5 cm x ~3 cm alveolar cleft defect was created by means of an oral surgery burr. An 4-week period followed this to allow for potential healing and to demonstrate that these defects were of a critical size.

At the conclusion of this interval, one of the rabbits received a computed tomography (CT) scan of the maxillofacial skeleton to allow for imaging of the alveolar cleft defect. This scan was used to design a customized, 3D-printable β-TCP scaffold using RoboCAD 4.3 (3D Inks LLC, Tulsa, OK). A rectangular scaffold matching the dimensions of the alveolar cleft defect was then created. To optimize its capacity for facilitating vascularized bone growth sought, an inner lattice network of cylindrical rods was designed with 500 µm-thick walls over the buccal and lingual surfaces to provide stability.

In a second surgical procedure, the alveolar cleft defects were exposed, soft tissue and bony speckles were trimmed, and a β-TCP scaffold was implanted in each rabbit. A 8-week period elapsed before each animal was euthanized and evaluated for bone formation in the defect site. This was done through microCT and quantitative analysis of 3D scaffold reconstructions using Amira 3D software (FEI, Hillsboro, Oregon).

Results: Bone formation within the alveolar cleft defect site was analyzed via 3D reconstruction with Amira 3D software. Analysis of the defects showed an average of 8.14% of osseous tissue occupying space within the scaffold-bone matrix to 91.86% scaffold. A trend of bone growth from the periphery towards the center of the scaffold was observed in most samples.

Conclusion: 3D-printed β-TCP scaffolds demonstrated limited osteoconductivity in alveolar cleft defects. A pattern of peripheral-to-central bone growth was evident on 3D reconstructions of the scaffold. This pilot study demonstrates the potential clinical value of this biomaterial-based therapeutic construct and indicates the importance of continued experimentation to fully assess its efficacy.

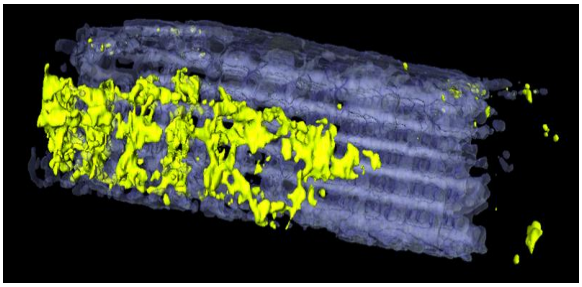

Figure 1: 3D reconstruction of scaffold showing peripheral-to-central pattern of bone growth

[1] Dixon M, Marazita M, Beaty T, Murray J. (2011). Cleft lip and palate: understanding genetic and environmental influences. *Nature Reviews Genetics.* 12(167-178).

[2] Murakami H, Nakasa T, Ishikawa M, Adachi N, Ochi M. (2016). Autologous bone grafts with MSCs or FGF-2 accelerate bone union in large bone defects. *Journal of Orthopedic Surgery and Research.* 11(105).

3D Printed Bioactive Ceramic Scaffolds for Critical-sized Mandibular Defects

Valerie Heredia[1], Christopher Lopez[1,2], J. Rodrigo Diaz-Siso[3], Jonathan Bekisz[4], Lukasz Witek[1], Eduardo Rodriguez[3], Paulo Coelho[1,3]

1. *Department of Biomaterials and Biomimetics, New York University College of Dentistry, New York, NY, USA*
2. *Icahn School of Medicine at Mount Sinai, New York, NY, USA*
3. *Hansjörg Wyss Department of Plastic Surgery, New York University Langone Medical Center, New York, NY, USA*
4. *New York University School of Medicine, New York, NY, USA*

Purpose: 3D printed scaffolds offer an alternative approach to large bony defect reconstruction. Rather than utilizing traditional grafting options such as nonvascular and vascular grafts, [1,2] in order to avoid donor site morbidity, infections, and other complications, synthetic biomaterials offer a novel approach. 3D bioactive ceramic-based scaffolds can also be customized to precisely defects. [3] This study uses a translational rabbit model to investigate the capability of the 3D printed scaffolds, composed of 100% β-TCP, to regenerate critical-sized mandibular ramus defects.

Methods and Materials: The study consisted of a total of fifteen (n=15) skeletally mature New Zealand white rabbits that underwent sterile surgical procedures in which a 10mm length x 10mm width x 3mm thickness mandibular ramus defect was created to insert the scaffold. Scaffolds were either control (uncoated), bovine collagen (COL) (2%) immersed, or dipyridamole/ collagen (COL-DIPY) immersed (100μM). Each rabbit received one of these three scaffolds. In order to allow time for healing, a time period of eight weeks followed after surgical procedures had taken place. After euthanizing animals, the rami were retrieved.

The rabbits were euthanized and rami extracted. Samples were dehydrated in a series of ethanol solutions and embedded in a methacrylate-based resin. After embedding, micro-computed tomography and 3D image reconstruction using Amira 6.1 software (Visage Imaging GmbH, Berlin, Germany) was performed. This software provided quantitative analysis of bone formation and scaffold resorption, at the same time it was capable of isolating desired areas (scaffold not surrounding ramus) by volume editing. The densities of bone and scaffold were isolated by thresholding and were quantified as percentages. After scanning, samples were cut into ~300um slices using a diamond saw (Isomet 2000, Buehler Ltd., Lake Bluff, IL, USA), and then polished using a grinding machine (Metaserv 3000, Buehler, Lake Bluff, IL, USA) to ~100 μm thickness. Samples were then stained to differentiate bone, scaffold and soft tissue by utilizing Stevenel's blue and Van Geison fuschin.

Results: The COL-DIPY group had the highest bone value (20.85%), as well as the lowest remaining scaffold percentage (79.15%) compared to the collagen and the control groups. The control group resulted in had the least scaffold resorption.

Conclusion: Insertion of scaffolds offers a novel approach to bony reconstruction that does not require harvesting any bony tissue from donor sites, which can avoid donor site morbidity. 3D printed bioactive ceramic based scaffolds merit further exploration.

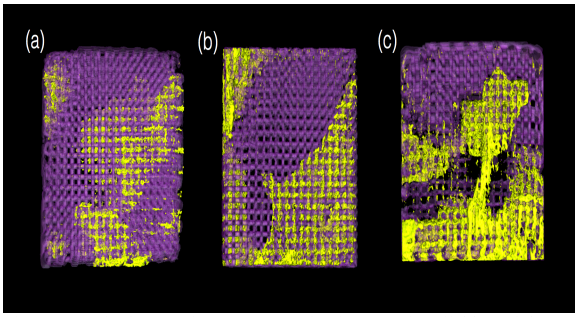

Figure 1: Amira image of 3D reconstruction images of scaffolds at eight weeks (a) Control, (b) Collagen and (c) DIPY/Collagen. DIPY/Collagen image shows the most bone regeneration in yellow.

References

1. Ivy RH. Iliac Bone Graft To Bridge a Mandibular Defect: Forty-Nine-Year Clinical and Radiological Follow-Up. Plastic and reconstructive surgery 1972;50:483-6.

2. Goldberg VM, Shaffer JW, Field G, Davy D. Biology of vascularized bone grafts. The Orthopedic clinics of North America 1987;18:197.

3. Warnke, P. H., Seitz, H., Warnke, F., Becker, S. T., Sivananthan, S., Sherry, E., Liu, Q., Wiltfang, J. and Douglas, T. (2010), Ceramic scaffolds produced by computer-assisted 3D printing and sintering: Characterization and biocompatibility investigations. J. Biomed. Mater. Res., 93B: 212–217

Insulin-like Growth Factor-1 Encourages Chondrocyte Chemotaxis and Cartilage Repair *In Vivo*

Margaret K. Boushell[(1)], Christopher Z. Mosher[(1)], Gurbani Suri[(1)],
Yelena Akelina[(1)], Clark T. Hung[(1)] Stephen Doty[(2)], Ernst B. Hunziker[(3)], Eric J. Strauss[(4)], Helen H. Lu[(1)]

1. Department of Biomedical Engineering, Columbia University, New York, NY, USA
2. Hospital for Special Surgery, New York, NY, USA
3. Department of Biomedical Engineering, University of Bern, Bern, Switzerland
4. NYU Langone Medical Center, New York, NY, USA

Disclosures: Margaret K. Boushell (none), Christopher Z. Mosher (none), Gurbani Suri (none), Yelena Akelina (none), Clark T. Hung (none), Stephen Doty (none), Ernst B. Hunziker (none), Eric J. Strauss (none), Helen H. Lu (none)

Keywords: Cell modulation, bioactive interface, in vivo, scaffold

INTRODUCTION: A variety of hydrogel-based cartilage grafts have been investigated for cartilage repair with promising results [1-6]; however, the integration of these grafts with host cartilage remains a translational barrier. Stimulating cell migration to the graft-cartilage boundary with chemotactic factors has been reported to improve integration with host cartilage [7].Thus, the objective of this study was to test the hypothesis that insulin-like growth factor (IGF-1) release from a fibrous scaffold will enable chondrocyte homing and promote graft-cartilage integration. To study the effect of IGF-1 release, a bovine full thickness defect model was used [8] and it was hypothesized that IGF-1 would promote healing at the host-graft cartilage junction.

METHODS: *Scaffold Fabrication & Characterization*: Unaligned microfiber scaffolds composed of a 5:1 blend of poly(lactide-co-glycolide) (85:15, Lakeshore) and poly(ε-caprolactone) (Sigma) were fabricated with and without IGF-1 (100 ng/mg) [9]. Fiber morphology was visualized using electron microscopy and IGF-1 release from the scaffolds was measured via ELISA (R&D Systems). *Cell migration:* Bovine cartilage explants (d=6 mm) were cultured atop scaffold disks with and without IGF-1 (n=5/group) for two weeks. Then cartilage explants were removed, the disks were stained with Calcein AM, imaged using confocal microscopy, and cell area (n=5) was quantified using ImageJ. *Cartilage Integration*: Using a custom mold, ring-shaped scaffolds were made with or without IGF-1 for use in the full thickness defect model described previously [8]. Immature bovine full thickness chondrocytes were mixed at a density of 10 million cells/mL in 2% low gelling agarose (Sigma) and pipetted into the defect (~100 µL) with or without a scaffold ring (n=3/group). Repaired explants (n=3/group) were then implanted subcutaneously in male athymic rats for four weeks (IACUC approved protocol). Matrix and cellularity at the host-graft junction were assessed histologically. *Statistical Analysis*: ANOVA and the Tukey-HSD test was used ($p<0.05$).

RESULTS: *Scaffold Characterization*: Meshes with and without IGF-1 exhibited similar morphology, with average fiber diameters of 1.2 ± 0.2 and 1.4 ± 0.1 µm, respectively. IGF-1 release from the fibers (n=4, Fig. 1) showed a burst release followed by sustained release. *Cell Migration*: After two weeks of culture (n=5), cells migrated from the explants onto each scaffold. Cells were randomly distributed on IGF-free scaffolds, but uniform with dense populations on IGF-containing scaffolds, mirroring the shape and size of the cartilage explant that was cultured atop. A significantly higher total sample fluorescence was measured for the IGF group with respect to the control ($p<0.05$). *Cartilage Integration*: GAG and collagen-rich tissue with aligned collagen fibers (Fig. 2) was observed at the host-graft junction for defects repaired with IGF-1 scaffolds. In contrast, fibrous gaps between the graft and host tissue were observed in sham defects.

DISCUSSION: The results of this study demonstrate that IGF-1 can be incorporated in fiber scaffolds, and home chondrocytes from host cartilage upon release. Further, when scaffolds are placed at the graft-host junction of a cartilage defect *in vivo*, a proteoglycan- and collagen-rich tissue is consistently deposited at the healing interface, while only incomplete healing occurs with sham repair. Future studies will focus on evaluation of the biomechanics of this novel integration strategy.

CONCLUSION: This study tackles the clinical hurdle of cartilage graft integration with surrounding host tissue. The results indicate that localized, controlled release of IGF-1 is a promising approach to stimulate cell migration to the graft-host junction and improve cartilage healing.

REFERENCES: [1] Jiang et al, 2010 [2] Holland et al, 2007 [3]Chao et al, 2010 [4] Mauck et al, 2000 [5]Khanarian et al, 2012 [6] Kim et al, 2011 [7] McGregor et al, 2011 [8]Boushell et al, 2014 [9] Moffat et al, 2009. ACKNOWLEDGEMENTS: We gratefully acknowledge the Columbia University ICM veterinary staff for their help with the rodent surgeries, including Rivka Shoulson, Samuel Baker, and Nicole Herndon. We also gratefully acknowledge Tony Labissiere and Orla O'Shea for their help with histological processing. This work was supported by NYSTEM and an NIH T32 training grant.

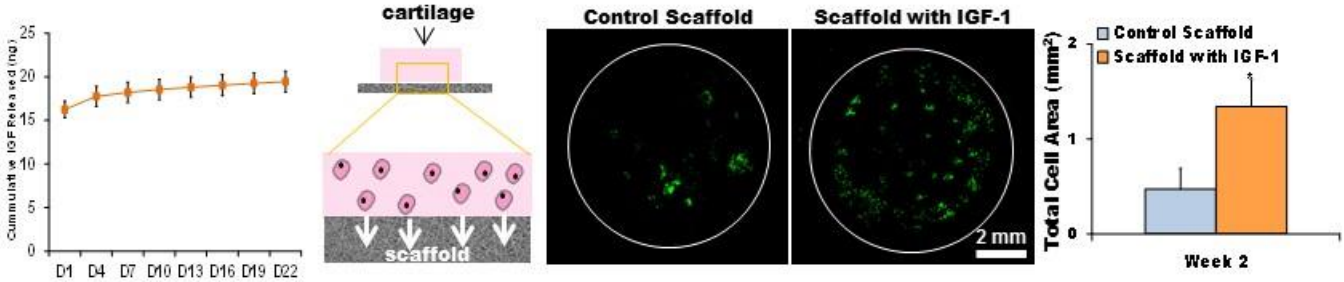

Fig 1. IGF-1 release from fibrous scaffolds measured via ELISA (n=4, left) increases cell migration from cartilage explants cultured atop the scaffolds (second from left) for two weeks as visualized with Calcein AM stain (third and fourth from left) and quantified via ImageJ (n=5, right).

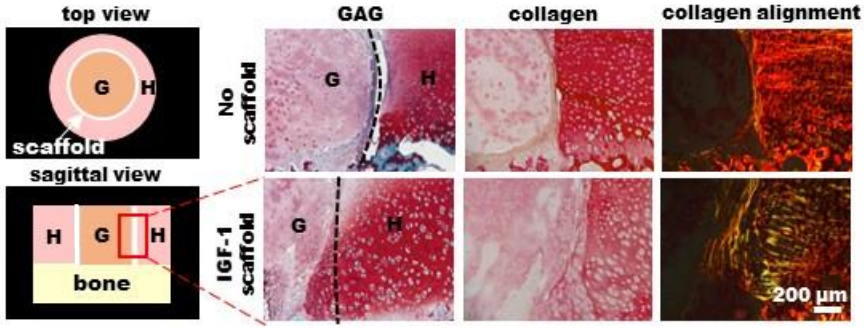

Fig 2. Integration with host cartilage. In this model (left), the presence of a fibrous scaffold that releases IGF-1 at the junction of the agarose graft (G) and host (H) cartilage results in increased deposition of GAG (second from left, safranin O) and collagen (third from left, picrosirius red)-rich tissue (bottom) when compared to control repair (top). Collagen alignment (right, polarized light microscopy of picrosirius red stained sections) is observed in defects repaired with the IGF-1 scaffold. (black dashed line traces healing interface)

SCREENING BIOACTIVE COMPOUNDS FOR THEIR PERIPHERAL NERVE REGENERATION POTENTIAL

Wei Chang PhD(1), Hilton M Kaplan MBBCh FCSSA PhD(1), Derek J Woloszyn BS(1), Matthew Richtmyer(1), Joachim Kohn PhD FBSE(1)

1. New Jersey Center for Biomaterials, Rutgers University, Piscataway, New Jersey

Abstract

Peripheral nerve injuries commonly lead to impaired sensation and motor function, particularly when large gaps occur, greatly affecting quality of life. It is still very challenging to treat peripheral nerve injuries. Using a nerve guidance conduit (NGC), as a “tube” to help the regenerating nerve cross the defect, has proven largely insufficient on its own. Therefore, in efforts to improve functional regeneration across large nerve gaps, the creation of a more conducive microenvironment is highly important. We have developed a “pump screening” protocol as a model for rapidly assessing potential neurotrophic factors for their ability to restore motor and sensory functions, quantitatively. The implanted pump system delivers drug into the full volume of the NGC over every 20 hours for 4 weeks. After an additional 2 weeks the NGC and repaired nerve stumps are harvested, and the degree of early regeneration is assessed histologically. Using this method, we are testing ten different substances, against negative and positive controls (no drug and brain-derived neurotrophic factor (BDNF), respectively). The current status of this project will be presented, and particularly the preliminary outcomes of two substances that show promise: Compound A that appears to have a protective effect on retrograde degeneration in the proximal stump; and Compound B that appears to promote nerve regeneration across the gap.

An Investigation of Glycosaminoglycan Mimetic Scaffolds for Axonal Growth

Roseline Menezes, Saba Bano, Bryan Pfister, Treena Livingston Arinzeh,
Department of Biomedical Engineering, New Jersey Institute of Technology, Newark, NJ, USA

Introduction: Injury to nervous tissue leads to severe dysfunction due to limitation in nerve regeneration. This is due to an inhibitory environment created at the site of injury. Neural tissue engineering using materials that closely mimic the extracellular matrix (ECM) during neural development could enhance neural regeneration. Glycosaminoglycans (GAGs), which are sulfated polysaccharides, have been shown to modulate axonal outgrowth in neural tissue depending upon the position and degree of sulfation. This study prepared aligned fibers of GAGs and GAG mimetics having varying levels and position of sulfation and evaluated their effect on axonal outgrowth.

Materials and Methods: Aligned fibers were prepared by electrospinning a solution of 24% (w/w) of gelatin (obtained from Bovine skin, Sigma) with 0.25% (w/w) of GAGs in 50:50 ratio of water and ethanol. Chondroitin 4-sulfate (CSA) and Chondroitin 6- sulfate (CSC) GAGs were used as controls since they are naturally occuring GAGs found in neural tissue. Two types of GAG mimetics, partially sulfated sodium cellulose (pNaCS), with sulfate groups predominantly on the 6 position, and fully sulfated sodium cellulose (NaCS), with sulfate groups on the 2,3 and 6 positions of the glucose unit, were used to study the effect of these mimetics on axonal growth. The blend of gelatin and GAG electrospun scaffolds were crosslinked using EDC-NHS. The scaffolds were characterized for alignment and fiber diameter using scanning electron microscopy (SEM). The scaffolds were placed in low attachment 96 well plates (n=9 for each scaffold). Dorsal root ganglion (DRGs) isolated from Sprague-Dawley rats were placed at the center of each scaffold and allowed to grow in DRG media for 4 days. The DRGs were later immunostained for neural filaments and imaged under confocal microscope. The images were analyzed for axonal growth using Adobe Photoshop and ImageJ software and statistical analysis was done using SPSS software for One Way ANOVA.

Results and Discussion: The fiber diameter was analyzed to be approximately 700nm (Figure 1.a.). The fibers showed approximately 80% alignment. The greatest axonal growth was detected on the scaffolds containing fully sulfated NaCS which was around 1.7mm long but was only statistically higher than gelatin and CSA scaffolds. Lower axonal length was detected for cells on scaffolds containing CSA, which was similar to studies reported by Wang et al.[1]There was no significant difference between the axonal growth on CSC and partially sulfated NaCS this could be due to fact that the carbohydrates are sulfated at 6th carbon in both of these polysaccharides, as well as CSC has shown to have a positive effect on the axonal growth of neurons as shown by Lin et al.[2] Overall it could be seen that there is different effect on neural outgrowth depending on the sulfation pattern of the GAGs.

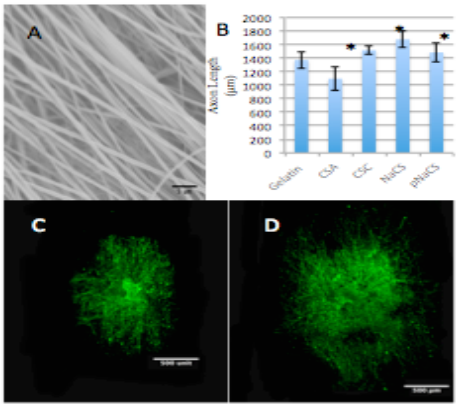

Figure 1. A. ***SEM image of electrospun aligned gelatin scaffold with 0.25% NACS (721.233±45.16 nm and alignment of 84%)(10,000X magnification). B.Axon length calculated on aligned gelatin scaffolds containing 0.25% of CSA, CSC and GAG mimetics with different sulfation levels. (n=9) (* p<0.05 significance in comparison to CSA; error bar shows ± standard error) C. Immunostained neurofilament on CSA (0.9mm average axon length) (10X magnification) D. Immunostained DRG for neurofilament on NaCS (1.6mm average axon length) (10X magnification)***

Conclusions: In conclusion we were successfully able to create aligned electrospun gelatin scaffolds containing various GAGs. Gelatin based scaffolds were able to sustain the DRG growth as well as able to provide contact guidance for axonal growth. The GAG mimetics were sucessfully able to enhance the axonal growth of these neurons and could be used for future neural tissue regeneration applications.

References: [1] Wang, H. J Cell Sci 121(2008): 3083–3091; [2] Lin, R. *PLoS ONE* 6 (2011): 1-10.

SprayBx: A Novel Biomaterial Spray for the Reduction of Post-Surgical Osteomyelitis

Shin-Jae Lee (1), Gunnar Mattson (2), Janani Narayan (3), Salvator Caruso (3), Sam Norwood (1,3), Connor Krill (1), Babar Shafiq (4), Lloyd Miller (5), and Hai-Quan Mao (1)

1. Department of Materials Science and Engineering, Johns Hopkins University, Baltimore, MD, USA
2. Department of Biomedical Engineering, Johns Hopkins University, Baltimore, MD, USA
3. Department of Chemical and Biomolecular Engineering, Johns Hopkins University, Baltimore, MD, USA
4. Department of Orthopaedic Surgery, Johns Hopkins Medicine, Baltimore, MD, USA
5. Department of Dermatology, Johns Hopkins Medicine, Baltimore, MD, USA

Post-surgical osteomyelitis (PSO) is a devastating complication following orthopedic procedures and is associated with very high return to surgery rates, resulting in longer hospital stays, higher mortality rates, and worse patient outcomes. PSO also has a significant financial impact on healthcare providers in the United States -- each year 35,000 patients contract orthopedic surgical site infections, which cost an estimated $150 million dollars to treat.

In an effort to reduce rates of infection, clinicians have begun to administer local antibiotics in addition to systemic prophylaxis, which has been shown to be effective, particularly for traumatic injuries. However, clinicians have expressed that the current standard for local prophylaxis, vancomycin powder, is a far from ideal delivery method, due to the fact that it is difficult to administer and, more importantly, because it does not offer a way to control release kinetics of the antibiotics.

We are developing a novel resorbable biomaterial spray, SprayBx, for the controlled delivery of antibiotics following orthopedic procedures, which will also provide significantly greater convenience and consistency than the current standard.

In order to offer clinicians as much control over the prophylaxis as possible, a combination of antibiotics is loaded into particles, which are carefully synthesized to release the drugs at a specific rate for a specific duration, which can be tuned based on patient needs. The particles are dispersed in a solution, which crosslinks to form a hydrogel matrix *in-situ* after being sprayed into the surgical site. The hydrogel matrix will ensure that the particles are retained at the site of the wound, minimizing potential side-effects.

Our current work involves characterizing antibiotic release from our spray in order to hone in on a synthesis method that results in release kinetics appropriate for the prevention of PSO. We are also fine-tuning our hydrogel matrix to achieve optimal mechanical properties, gelation, and degradation. Finally, we have begun to quantify the benefits of SprayBx over vancomycin powder.

In conclusion, SprayBx will give clinicians a convenient antibiotic delivery device, which, through greater control over antibiotic release, will reduce rates of post-surgical osteomyelitis and, ultimately, other surgical site infections. In the long-term, SprayBx can be modified for a variety of applications ranging from injectable antibiotic therapy to implant coatings.

The effect of human cryopreserved viable amniotic membrane on the biofilm formation by *P.aeruginosa*

Anya Singh-Varma[1], Yong Mao[1], Tyler Hoffman[2], Alla Danilkovitch[2] and Joachim Kohn[1]

[1] *New Jersey Center for Biomaterials, Rutgers University, 145 Bevier Rd., Piscataway, NJ 08854*
[2] *Osiris Therapeutics, Inc. Columbia, MD 21046*

Biofilms, a population of bacteria grown within self-produced extracellular polymeric substances, are often resistant to antibiotic treatment and remain as one of the key challenges in treating chronic wounds. A recent clinical study showed that human cryopreserved viable amniotic membrane (hCVAM) promoted closure of chronic diabetic foot ulcers and reduced wound-related infections [1]. The intrinsic antimicrobial activity of hCVAM against a spectrum of wound-associated pathogens under planktonic (floating) culture condition was also demonstrated in an *in vitro* study [2]. Such activity is most likely attributed to antimicrobial peptides produced by the viable cells in hCVAM [3]. The goal of this study is to evaluate the effect of hCVAM on the formation of biofilms by *P. aeruginosa*, a pathogen commonly associated with chronic wounds. In this study, the formation of biofilms on polystyrene surface and dermal tissue surface were evaluated. In order to avoid the physical disturbance of hCVAM on the biofilm formation, we prepared conditioned medium from hCVAM. The *P. aeruginosa* was inoculated to conditioned medium or assay medium (a control) in wells of a polystyrene plate. The plates were incubated for 48 h, and after that, gentamicin was added to the wells at 20x MIC (minimal inhibitory concentration) for 24 h to eliminate the planktonic bacteria. The biofilms in the wells of the polystyrene plates were washed and stained with crystal violet. We demonstrated that the formation of biofilm was significantly reduced when *P. aeruginosa* was inoculated in hCVAM conditioned medium compared to the control assay medium. In addition, we adapted a wound-relevant porcine dermal biofilm model [4] to confirm the effect of hCVAM on the biofilm formation. Pieces of porcine dermis were soaked in the hCVAM conditioned medium or assay medium for 6 h. The *P. aeruginosa* was inoculated onto the dermal tissues lying on agar plates. After incubation for 72 h and the removal of planktonic bacteria, the *P. aeruginosa* in the biofilm was extracted and quantified by serial dilution and CFU counting. We observed the inhibition of biofilm formation on dermal tissue in the presence of hCVAM-derived conditioned medium. Altogether, our results demonstrate that hCVAM has antimicrobial activity inhibiting *P. aeruginosa* biofilm formation.

[1] Lavery, L. A., Fulmer, J., Shebetka, K. A., Regulski, M., Vayser, D., Fried, D., Kashefsky, H., Owings, T. M., Nadarajah, J., and Grafix Diabetic Foot Ulcer Study, G. (2014) The efficacy and safety of Grafix((R)) for the treatment of chronic diabetic foot ulcers: results of a multi-centre, controlled, randomised, blinded, clinical trial, *Int Wound J 11*, 554-560.

[2] Mao, Y., Hoffman, T., Johnson, A., Duan-Arnold, Y, Danikovitch, A., Kohn, J. (2016) Human cryopreserved viable aminotic membrane inhibits the growth of bacteria associated with chronic wounds, *Journal of Diabetic Foot Complications 8*, 23-30.

[3] Mao, Y., Hoffman, T., Singh-Varma, A., Duan-Arnold, Y, Danikovitch, A., Kohn, J. (2017) Antimicrobial Peptides Are Responsible for the Antimicrobial Activity in a Human Cryopreserved Viable Amniotic Membrane *Manuscript in preparation*.

[4] Phillips, P. L., Yang, Q., Davis, S., Sampson, E. M., Azeke, J. I., Hamad, A., and Schultz, G. S. (2015) Antimicrobial dressing efficacy against mature Pseudomonas aeruginosa biofilm on porcine skin explants, *Int Wound J 12*, 469-483.

Viscous polymeric biomaterials for ocular drug delivery

Shiyu Xia (1, 2), Qingguo Xu (1, 3), Justin Hanes (1, 2, 3)

1. Center for Nanomedicine, Johns Hopkins School of Medicine, Baltimore, MD, USA
2. Department of Ophthalmology, Johns Hopkins School of Medicine, Baltimore, MD, USA
3. Department of Chemical and Biomolecular Engineering, Johns Hopkins University, Baltimore, MD, USA

Introduction: While drug-loaded microparticles (MP) can serve as drug reservoirs for sustained drug release, needle clogging by MP poses a challenge for ocular drug delivery. Biomaterials including hyaluronic acid (HA) and methylcellulose (MC) have been tested for their applicability for ocular injections. HA and MC were physically blended with drug-loaded polymeric MP for subconjunctival (SC) injection into rat eyes. The HA and MC viscous solutions facilitated injection through fine-gauged needles due to their shear-thinning properties. The diffusion barrier presented by HA and MC extended the drug release from MP. The significant level of MP retention in the conjunctiva tissue post operation affirmed the minimal leakage of MP following injection. The safety of HA and MC for ocular applications was demonstrated histologically.

Experimental methods: Model drug-loaded PLGA MP were prepared using single emulsion and solvent evaporation. Diameters of MP were characterized using a Multisizer 4e Coulter Counter, surface charge by laser doppler anemometry using a Zetasizer Nano ZS90. SEM images of drug-loaded PLGA MP were obtained from LEO/Zeiss Field-Emission scanning electron microscope. Rheology studies of HA and MC were conducted on an ARES RFS III rheometer. All animal procedures, including ocular retention study and histological examination, followed the regulations of the Johns Hopkins Animal Care and Use Committee and the Association for Research in Vision and Ophthalmology (ARVO).

Results: Viscous biomaterials HA and MC were rheologically shown to facilitate SC injection of concentrated suspensions of PLGA MP. HA and MC viscous solutions remarkably improved the injectability of MP, exhibited high retention of MP post-injection, induced minimal injection-related inflammation, reduced burst drug release and extended overall release. The results are partially summarized in Figure 1.

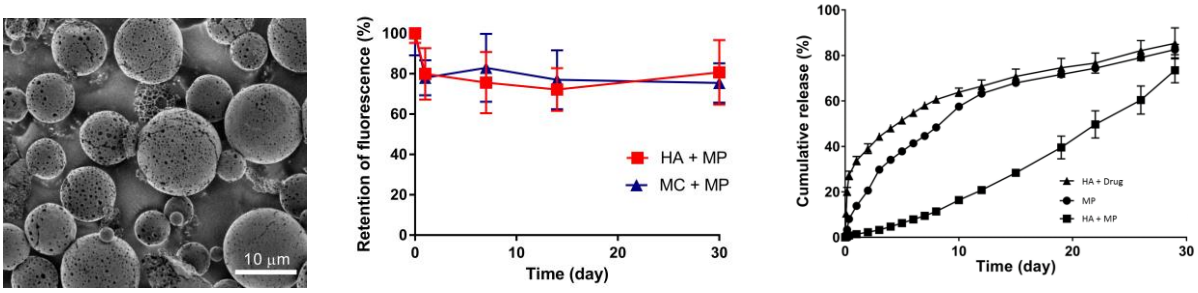

Figure 1. SEM image of PLGA-MP (left); in vivo retention study (middle); in vitro drug release assay (right).

Acknowledgement: The authors are grateful to the Sharon Gerecht Lab for help with rheometer operation, and thankful for Maria Jose Suarez for help with histology imaging. The Johns Hopkins University Office of the Provost supported this study.

Footnotes: Intellectual and commercial properties of Justin Hanes Lab and Johns Hopkins University; manuscript in preparation and review for publication.

Cell Type Influences Local Delivery of Biomolecules from a Drug Delivery System

J. Alhamdi(1,2), E. Jacobs(1,2), M. Hurley(1), G. Gronowicz(1) , L.T. Kuhn(1,2)
1. Reconstructive Sciences, University of Connecticut Health, Farmington, CT, USA
2. Biomedical Engineering, University of Connecticut, Storrs, CT, USA

Statement of Purpose: Sequential delivery of multiple factors is essential to mimic several different steps of tissue regeneration. This study investigated how cell type influenced sequential delivery of factors from a biomimetic calcium phosphate-polyelectrolyte multilayer (bCaP-PEM) coating delivering fibroblast growth factor-2 (FGF-2 or F) followed by antimycin-A (AntiA or A) (Figure 1). The aim was to study the mechanism used by each cell type to access the factors embedded in the coating.

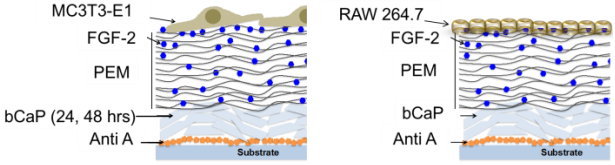

Fig. 1. MC3T3-E1 or RAW264.7 cells were tested on bCaP-PEM coatings delivering two biomolecules.

Methods: bCaP coating: Sandblasted tissue culture plastic disk inserts were coated with bCaP layers using a simulated body fluid method (SBFx5) [1]. bCaP thickness was changed by increasing the time in the SBFx5 solution from 24 to 48 h. **PEM bilayer coating:** PEM bilayers were applied to bCaP coated disks by automated dipping in poly-L-Glutamic acid (PLGlut) or poly-L-Lysine (PLLys) solutions with saline rinses in between [2]. **Factor Application:** A cytotoxic factor antimycin A (AntiA) was adsorbed directly on the disk and then covered with the bCaP layer (Fig. 1). A cell proliferative factor, FGF-2 was adsorbed into the PEM layers (Fig.1). **Cell Culture and Analysis:** MC3T3-E1 mouse calvarial osteoprogenitor cells were seeded at $4x10^4$ cells/cm^2, cultured in α-Minimal Essential Medium, with 10% FBS and 1% pen/strep. RAW 264.7 macrophages were seeded at 3 x 10^4 cells/cm^2 in DMEM high glucose with 10% FBS, and 1% pen/strep. LIVE® staining and imaging was used to quantify proliferation from FGF-2 and cytotoxic effects from accessing AntiA. SEM was used to study degradation of coating structure by cells over time. **Results:** MC3T3-E1 accessed the embedded AntiA after a 3 days delay when cultured on bCaP (24hr)-PEM (Fig 2). For bCaP(24) coating only without PEM, cells began gradually accessing the AntiA after 2 days of culture (Fig. 2). Depositing a thicker bCaP layer (48 h) with PEM slightly delayed the delivery of AntiA; however, bCaP(48) without PEM did not increase MC3T3-E1 access time to the second factor AntiA indicating PEM is an important component of the delivery system.

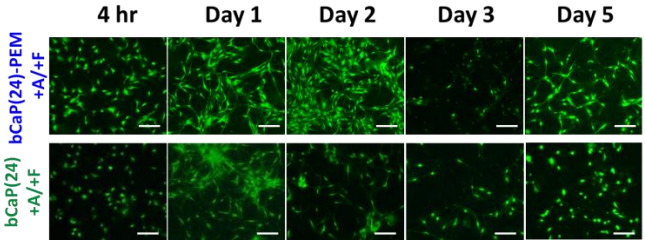

Fig. 2. LIVE® stained area of MC3T3-E1s over time.

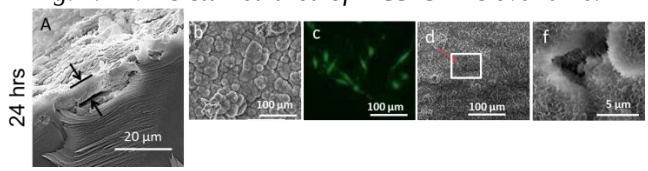

Fig 3. A) SEM cross-section of bCaP(24) coating thickness=6 µm. b) bCap before cell culture, c) Day-3 LIVE staining +A/+F bCaP24-MC3T3-E1, d, f) bCap after 3 days of cell culture.

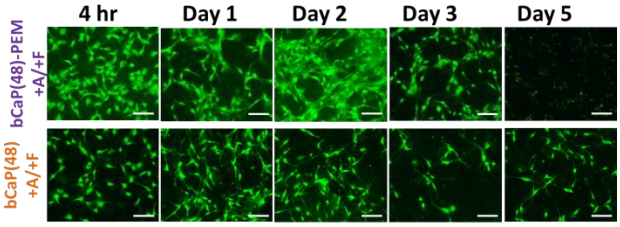

Fig. 4. Cell viability on bCaP(48)-PEM and bCaP(48)

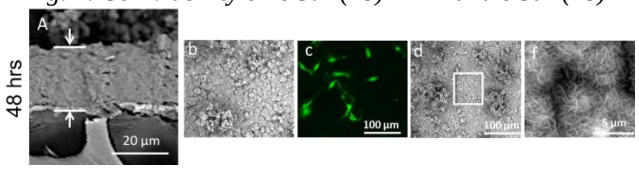

Fig 5. A)SEM cross-section of bCaP(48) coating thickness=24 µm. *b) bCap-48 before cell culture, c) LIVE staining +A/+F bCaP48-MC3T3-E1, d and f)bCap-48 after 3 days of cell culture*

The RAW264.7 cells immediately accessed the embedded AntiA on bCaP(24)-PEM and RAW264.7 cells accessed AntiA after a 3 days delay on bCaP(24) only (Fig 5).

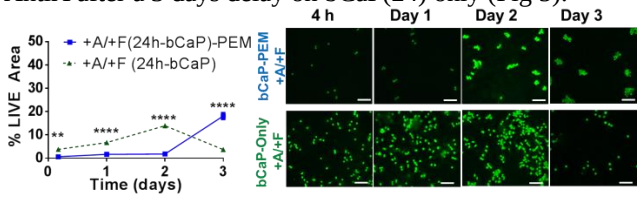

*Fig. 5. Percent LIVE® stained area of RAW 264.7 cells. ** $p \leq 0.01$, **** $p \leq 0.001$.*

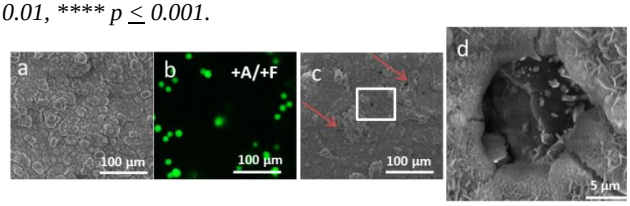

Fig. 6 A) bCap before cell culture, B) +A/+F-bCaP-Raw cells, c and d) bCaP coating after three days of RAW cells culture.

Discussion and Conclusions: The bCaP-PEM system is capable of sequential delivery of two active biological factors. Delivery kinetics is cell dependent and varies depending on the cells ability to either enter through microcracks the bCaP coating or dissolve it. The RAW 264.7 macrophage-like cells accessed the embedded factor below the coating faster than the MC3T3-E1 cells. This fast access by RAW cells is due to their ability to quickly dissolve the coating. The RAW cells created a micro-opening by dissolving the bCaP coating (Fig. 6), while MC3T3-E1 penetrated through cracks in the coating to get access to AntiA (Fig.3). Cell type should be considered when designing growth factor delivery systems. Cell access and kinetics will be studied further.

References: [1] Goldberg AJ, Kuhn LT et al. J Biomat Sci Polymer, 2010;21:1371-87. [2] E.Jacobs, Kuhn LT et al. J Biomat,10.1002.

Self-Assembled Micelle Enables Effective CRISPR/Cas9 Delivery for Human Papillomavirus Oncogene Disruption

Yeh-Hsing Lao, [1] Mingqiang Li,[1] Madeleine A. Gao[1] and Kam W. Leong[1,2]*

[1]Department of Biomedical Engineering, Columbia University, New York 10027, NY
[2]Department of Systems Biology, Columbia University Medical Center, New York, 10032, NY
*corresponding author: kam.leong@columbia.edu

As an RNA-guided nuclease, CRISPR-associated protein 9 (Cas9) enables precise, programmable DNA interference, and it has become a transformative tool for gene editing since its discovery. However, safe and efficient delivery of Cas9 nuclease and its counterpart, guide RNA (gRNA), remains unsatisfactory; especially for non-viral Cas9 plasmid delivery, the reported efficiency is limited, even with the widely-used liposomal carrier, Lipofectamine. In this study, we report a new self-assembled micellar system, comprising quaternary ammonium-terminated poly(propylene oxide) (PPO-NMe_3) and amphiphilic Pluronic F127, optimized for this application (**Figure 1A**). We evaluated this design on a human cervical cancer model. With the optimized formulation, this micelle was superior on Cas9 transfection with lower cytotoxicity, compared with the two well-characterized carriers, polyethylenimine and Lipofectamine. To assess the efficacy, we designed two gRNA/Cas9 all-in-one constructs to target the human papillomavirus (HPV) E7 oncogene, known to inhibit retinoblastoma protein through the ubiquitin-proteasome pathway and cause abnormal cell proliferation (**Figure 1B**). In conjunction with the most potent E7-targeting gRNA-/Cas9-encoded construct, the micelle was able to suppress the downstream protease activity by 31.9 ± 11.2% and thus inhibited the cervical cancer cell proliferation, only reaching 68.1 ± 9.53% cell viability of the Cas9 control. We further sorted the transfected cells and confirmed the gene disruption by T7 endonuclease I assay and Sanger sequencing. More than half (52.1%) of the micelle-transfected clones' E7 oncogene was disrupted, while only 26.1% of Lipofectamine-transfected clones showed this oncogene disruption. Taken together, the proposed micellar system holds the potential for the genome editing application and may add to the armamentarium of cancer nanomedicine.

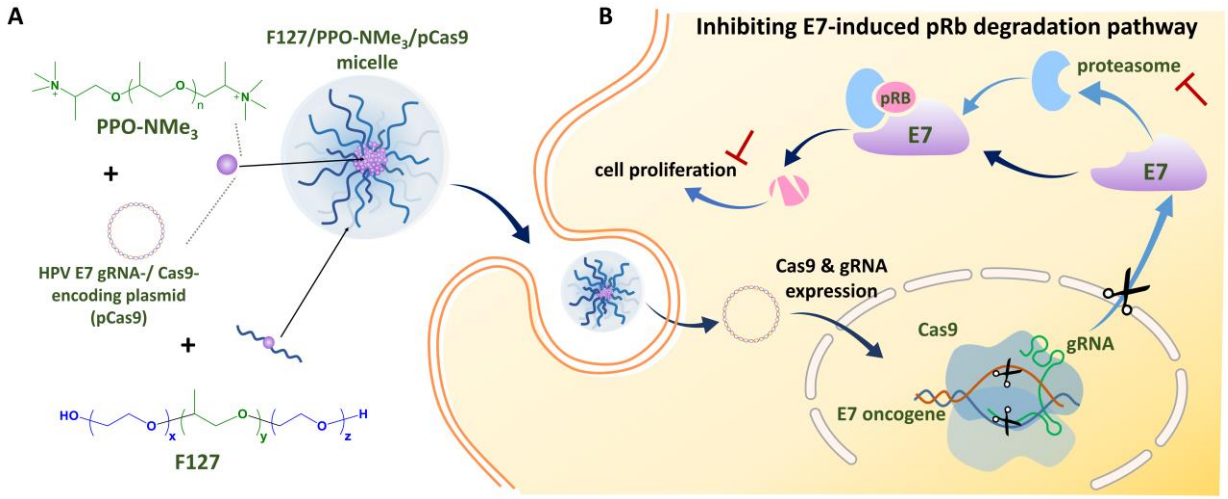

Figure 1. (A) Design of the proposed micellar system and (B) its mechanism on HPV E7 disruption.

Mesenchymal stem cells coated with graphene oxide for cancer therapy

S.Suryaprakash,[1] K.Leong [1]
[1] Columbia University in the City of New York, NY, USA

Abstract:
Graphene based systems have widely been used as a carrier for cancer therapy[1]. However most of the targeting is through passive targeting, stem cells such as mesenchymal stem cells on the other hand, have inherent tumor tropic properties that makes them an attractive cellular delivery vehicle for cancer therapy[2]. We have developed a new system where graphene oxide (GO) loaded with drugs is used to coat the surface of the mesenchymal stem cells, and the mesenchymal stem cells carries the GO-Drug composite directly to the site of tumor (Fig 1A). This system allows us to take advantage of MSCs unique tumor trophic properties, and simultaneously GO's ability to load a wide variety of drugs including proteins, nucleic acids, and small molecules.

We have been able to show that GO is not toxic to the MSC during long-term incubation. The GO can coat the surface of the MSC as demonstrated through scanning electron microscope, and fluorescent microscope (Fig 1B).

The GO coated MSC can successfully migrate towards the tumor cells within 24 hrs at a velocity equivalent to normal MSCs carrying the GO along with it(Fig 1C). GO loaded with doxorubicin (GO-DOX) and GO loaded with metoxantrone (MTX) were tested against a wide range of cancer drugs and were able to preferentially kill the cancer cells leaving MSCs unharmed. We then coated the MSC with GO-DOX and GO-MTX composite and co-cultured with LN18 a glioblastoma cell line. The co-culture of MSC carrying the drugs and cancer cells resulted in dose dependent killing of the LN18 cells demonstrating the killing efficiency.

MSC-GO is an efficient drug delivery system that can migrate towards the site of the tumor and deliver a wide range of therapeutics locally to kill the cancer cells. We plan to use to the system to test the efficacy in vivo in the future.

Keywords: Graphene oxide, cancer, stem cells, glioblastoma, cancer therapy, drug delivery

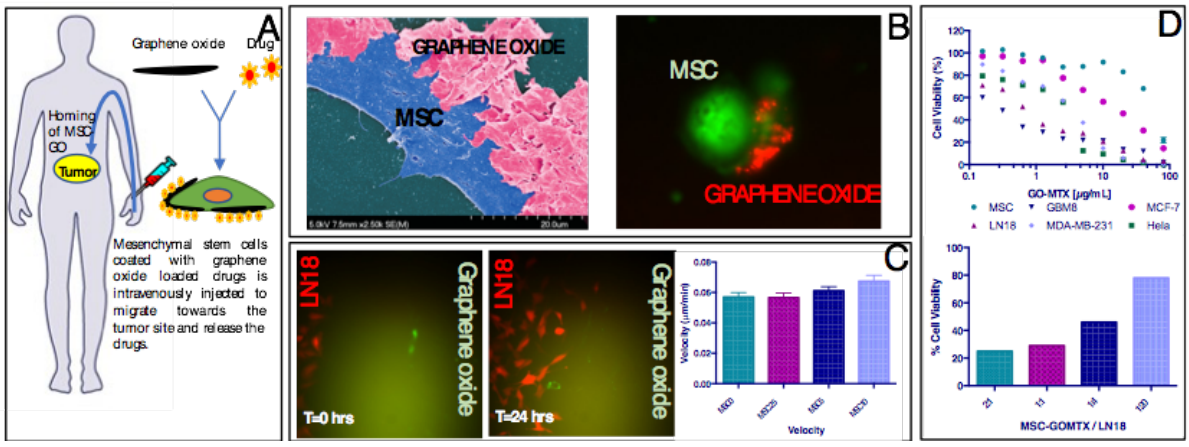

Figure 1: Figure (1A) MSC coated with graphene oxde loaded drugs migrate towards the site of tumor to release drugs locally. (1B) SEM and fluorescent images of GO coating on the surface of MSC. (1C) Migration of MSC coated with GO towards cancer cell in 24 hrs. (1D) Toxicity of GO-MTX on cancer cells and co-culture of MSC-GO-MTX with cancer cells showing dose dependent toxicity.

References:

1. Kundu, A., Nandi, S., Das, P. & Nandi, A. K. Fluorescent Graphene Oxide via Polymer Grafting: An Efficient Nanocarrier for Both Hydrophilic and Hydrophobic Drugs. *ACS Appl Mater Interfaces* **7,** 3512–3523 (2015).
2. Shah, K. Mesenchymal stem cells engineered for cancer therapy. **64,** 739–748 (2012).

Introduction: There is a need for materials to improve outcomes following trauma to soft tissue associated with numerous conditions including combat injury, tumor excision or diabetes. Hydrogels with anti-inflammatory properties are potential candidate materials for such clinical indications, and may aid in the healing process. Methylcellulose (MC) hydrogels have been shown to serve as stable injectable fillers[1][2][3], but do not possess inherent wound healing properties. Curcumin is an active component of the spice turmeric with multiple reported therapeutic attributes, including anti-inflammatory and anti-cancer activity.[4] In this study, curcumin was incorporated into injectable MC hydrogels, and the mechanical and physical properties of the gels were investigated together with the curcumin release profile.

Materials and Methods: A combination of MC (14kDa:41kDa, 1:1) polymer methacrylated at ~9% was prepared as previously described.[1][2][3] Methacrylated MC was dissolved in PBS at concentrations of 1%, 2%, and 3% (wt/vol) and combined with ammonium persulfate (APS) and ascorbic acid (AA) free-radical initiators at 10 mM each, and cast in cylindrical molds using a dual-barrel syringe. Curcumin-loaded gels (MC_{curc}) were prepared with 50 µg/mL curcumin. Confocal microscopy was used to visualize the curcumin-encapsulated hydrogel network. The equilibrium Young's modulus (Ey) was measured in unconfined compression and the equilibrium weight swelling ratio and other physical properties (mesh size, crosslinking density) were calculated as previously[1][2][5]. Cytocompatibility was assessed by co-culture with human dermal fibroblasts based on DNA measurements and live/dead staining. Curcumin release was measured from gels immersed in PBS at 37℃. The concentration of curcumin was quantified fluorometrically at an excitation wavelength of 450 nm and emission wavelength of 535 nm.[6] The diffusion coefficient was measured based on prior studies[7] and gels were imaged with a stereomicroscope to visualize the temporal change in curcumin intensity.

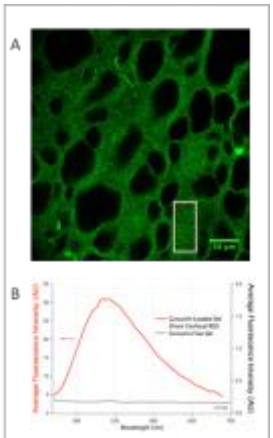

Fig. 1 (A) Representative confocal fluorescence microscopy image of a curcumin-loaded MC hydrogel ($MC_{curc,2\%}$) displaying the porous polymer network with incorporated curcumin throughout the structure. (B) Spectral imaging analysis of the region of interest (white box in C) of the curcumin-loaded gel indicates a peak fluorescence intensity corresponding to the characteristic emission maxima of curcumin (~540 nm), which was not observed in curcumin-free gels.

Results and Discussion: Curcumin incorporated into the MC_{curc} gels was uniformly distributed throughout the polymer network, as shown via confocal imaging.Consistent with the theory of rubber elasticity and with previous work, swelling properties displayed an inverse relationship to macromer concentration; $MC_{curc,1\%}$ hydrogels exhibited the highest swelling ratio and mesh size, and lowest crosslinking density, which was significantly different from the $MC_{curc,2\%}$ and $MC_{curc,3\%}$ gels. By varying macromer concentration, the Ey ranged between 2.06±1.60 and 4.32±1.15 kPa, for $MC_{curc,2\%}$ and $MC_{curc,3\%}$ hydrogels, and 4.71±2.15 and 8.93± 3.04 kPa for $MC_{2\%}$ and $MC_{3\%}$ gels, respectively. These values were on par with human adipose tissue[8] ($MC_{1\%}$ gels were too weak for mechanical testing). Live/dead staining showed robust cell viability, which was confirmed by DNA content of the cells in co-culture with MC or MC_{curc} gels. Cumulative release was monitored for 2 weeks, with the bulk of curcumin released by 48 hours. Release was lowest in the $MC_{curc,3\%}$ gels, which also displayed the significantly lowest diffusion coefficient.

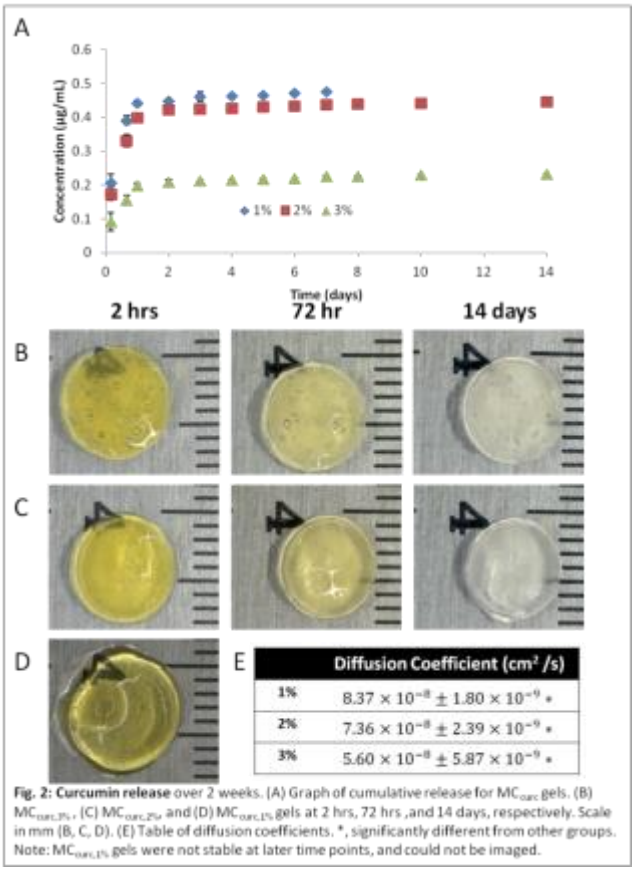

Fig. 2: Curcumin release over 2 weeks. (A) Graph of cumulative release for MC_{curc} gels. (B) $MC_{curc,3\%}$, (C) $MC_{curc,2\%}$, and (D) $MC_{curc,1\%}$ gels at 2 hrs, 72 hrs ,and 14 days, respectively. Scale in mm (B, C, D). (E) Table of diffusion coefficients. *, significantly different from other groups. Note: $MC_{curc,1\%}$ gels were not stable at later time points, and could not be imaged.

Conclusion: Taken together, curcumin-loaded MC hydrogels polymerized using a redox crosslinking system have potential for various clinical indications requiring soft tissue reconstruction. The therapeutic effect of curcumin delivery from MC hydrogels will be investigated in the future.

References:[1] Gold, G. T. et al. Injectable Redox-Polymerized Methylcellulose Hydrogels as Potential Soft tissue Filler Materials. J. Biomed. Mater. Res. A 102, 4536–4544 (2014). [2] Gold, G. T., Varma, D. M., Taub, P. J. & Nicoll, S. B. Development of crosslinked methylcellulose hydrogels for soft tissue augmentation using an ammonium persulfate-ascorbic acid redox system. Carbohydr. Polym. 134, 497–507 (2015). [3] Stalling, S. S., Akintoye, S. O. & Nicoll, S. B. Development of photocrosslinked methylcellulose hydrogels for soft tissue reconstruction. Acta Biomater. 5, 1911–1918 (2009). [4] Hatcher, H., Planalp, R., Cho, J., Torti, F. M. & Torti, S. V. Curcumin: From ancient medicine to current clinical trials. Cell. Mol. Life Sci. 65, 1631–1652 (2008). [5] Varma, D. M., Gold, G. T., Taub, P. J. & Nicoll, S. B. Injectable carboxymethylcellulose hydrogels for soft tissue filler applications. Acta Biomater. 10, 4996–5004 (2014). [6] Shpaisman, N., Sheihet, L., Bushman, J., Winters, J. & Kohn, J. One-Step Synthesis of Biodegradable Curcumin-Derived Hydrogels as Potential Soft Tissue Fillers after Breast Cancer Surgery. Biomacromolecules 13, 2279–2286 (2012). [7] Leach, J. B. & Schmidt, C. E. Characterization of protein release from photocrosslinkable hyaluronic acid-polyethylene glycol hydrogel tissue engineering scaffolds. Biomaterials 26, 125–135 (2005). [8] Samani, A., Zubovits, J. & Plewes, D. Elastic moduli of normal and pathological human breast tissues: an inversion-technique-based investigation of 169 samples. Phys. Med. Biol. 52, 1565–1576 (2007).

Engineering a drug-eluting stent to treat laryngotracheal fibrosis

Madhavi Duvvuri (1,2), Kevin Motz, MD (1,2), Michael K. Murphy, MD (1,2), Alexander T. Hillel, MD (1,2)

1. Department of Biomedical Engineering, Johns Hopkins University School of Medicine, Baltimore, MD, USA.
2. Department of Otolaryngology-Head and Neck Surgery, Johns Hopkins University School of Medicine, Baltimore, MD, USA.

Background: Laryngotracheal fibrosis occurs in 10% of patients who have been intubated. Due to an immune-mediated response, scarring of the glottis, subglottis and the trachea can occur, resulting in dysphonia, aphonia as well as airway occlusion, which requires subsequent surgeries to repair. Having previously shown the effect of rapamycin on reducing fibrosis in vitro, our goal was to develop a rapamycin-eluting stent that has a reliable drug-release profile and is mechanically durable so that it can be used to prevent fibrosis after initial intubation injury.

Methods: Biodegradable and biocompatible stents made of PLLA-PCL (70 % Poly-L-Lactide and 30% Polycaprolactone blend) and 50:50 PDLGA (Poly(DL-lactide-co-glycolide)) were fabricated using a glass mold. Rapamycin was incorporated into the polymer solutions before the stents dried in a vacuum. Stents were placed in a transwell culture dish in PBS at 37^{o}C and 5% CO_2 to mimic biological conditions. Elution method and high performance liquid chromatography analysis (HPLC) was used to characterize rapamycin release profiles for each stent. Compression and tensile strength testing were completed using a rheometer to determine the mechanical characteristics of each stent. Finally, a stent for a mouse trachea was fabricated to be placed into the mouse using a sialendoscope.

Results: The PLLA-PCL stent exhibited greater mechanical strength compared to the PDLGA stent, whereas over 4 weeks, the PDLGA stent became brittle and disintegrated under simulated biological conditions. Moreover, the PLLA-PCL stent showed a reliable rapamycin release profile for 6 weeks. The PLLA-PCL stent was also placed successfully into the mouse: the first time a mouse model has been used to test a stent-based drug delivery system to the trachea.

Conclusions: We demonstrate that PLLA-PCL biodegradable stents showed superior mechanical strength and rapamycin release for 6 weeks compared to PDLGA stents. We also placed a drug-eluting stent in a mouse for the first time.The biodegradable rapamycin-eluting PLLA-PCL stent shows promise in being used to treat laryngotracheal fibrosis in future translational studies. We are currently conducting translational experiments in a bleomycin-induced mouse model of LTS and fibroblast cell cultures to assess the effect of this rapamycin-eluting stent in reducing fibrosis in vitro and in vivo.

DNA ChemoFilter: A Novel Method to Prevent Systemic Toxicity from Intra-Arterial Administration of Chemotherapeutics

PURPOSE

While chemotherapy has revolutionized treatment of cancer, chemotherapeutics result in significant systemic toxicity, thus limiting use of highly effective drugs. Intra-arterial administration of drugs directly to the tumor has been a promising way to limit systemic toxicity, while at the same time administering high drug doses. This method has been widely used in treatment of liver cancer, but 50-70% of administered chemotherapeutics can bypass the tumor and still enter the systemic circulation, resulting in systemic toxicity that leads to renal failure, cardiac failure, and more harmful side ffects(Porrata et. Al, 2001). Thus, we developed the ChemoFilter, a device that aims to allow administration of high dose of chemotherapeutics directly to the tumor, while limiting the amount of drug that bypasses the tumor. We propose a new method of filtration with the ChemoFilter using immobilized DNA to bind chemotherapeutics that contain intrinsic DNA binding activity.

METHOD AND MATERIALS

We performed DNA binding experiments in vitro with Doxorubicin and PBS solution, and genomic DNA was used to determine optimal binding kinetics. Binding kinetics in nylon mesh of different pore size were also evaluated.

RESULTS

The DNA ChemoFilter decreases Doxorubicin concentration from solution *in vitro* by more than 90% within 1 minute. DNA demonstrates more rapid and efficient binding kinetics than a previously tested ion-exchange resin. Furthermore, when DNA was sequestered with nylon and polyester mesh, there was a 70% clearance of Doxorubicin from solution within 5 minutes.

CONCLUSION

The DNA ChemoFilter rapidly binds to Doxorubicin and clears chemotherapeutics with intrinsic DNA binding from solution. Future steps include in vivo trials and modifying the design of the device to maximize Doxorubicin clearance within solution. We are currently working on adapting this device to chemotherapeutics such as Cisplatin and antibiotics including Gentamicin, in the effort to reduce systematic toxicity that results from delivery of chemotherapeutics.

Title:Solid Tumor Analogues: Properties affecting the penetration of liposomes and their contents

Authors and Mentors: Varun Khandavalli (1), Timothy Mahon (1), Thomas Baker (1), Anand Arikarevula (1), Dr. Stavroula Sofou (1), Michelle Sempkowski (1), Sally Stras (1)

Abstract:

Our project, titled Solid Tumor Analogues: Properties Affecting the Penetration of Liposomes and their Contents, is focused on understanding and developing a model of a new drug delivery system that can enhance penetration of a drug within a solid tumor. There are many challenges associated with drug carriers and their ability to control tumor growth. Several factors limit the penetration a drug and its carrier have inside a solid tumor. While a sufficient amount of drug may be delivered to a tumor, factors which cause limited penetration reduce the ability to effectively kill cancer cells. By engaging in heterogenous distribution, certain cancer cells are in contact with excessive amounts of drug, while other cells never interact with the drug. Furthermore, many drug delivery systems face slow diffusion across a tumor but fast blood clearance, thereby amplifying this issue. Our project seeks to incrementally overcome these challenges by focusing on increasing penetration of a drug and allowing for a more homogenous distribution. Two major features of drug delivery carriers are targeting of a tumor and release of the drug.

To address both issues of limited penetration and slow diffusion across a tumor, we propose to use pH-sensitive liposomes. The goal of using ph-sensitive liposomes is to create a way for a drug delivery carrier to have greater release of drug at the tumor site, while still maintaining the same drug retention as ordinary liposomes, in other areas of the body. Research on ph-sensitive liposomes had been conducted by our mentor, Dr. Sofou, and her group for quite some time. pH responsive liposomes, can be introduced into the body, and will function autonomously. Other drug delivery carriers are being developed to improve drug penetration within a tumor, however many of these drug delivery systems require the use of other drugs, heat, or infrared light for proper release at the tumor.

1. Department of Biomedical Engineering, Rutgers University, Piscataway, NJ, USA

Title: Self-assembling, enzyme-responsive peptides for improved doxorubicin targeting

Authors: Denise Robles (1); Jiye Son (2,3); Rein Ulijn, Ph.D. (3)

Affiliations: 1. City College of New York
2. Graduate Center of the City University of New York (CUNY)
3. CUNY Advanced Science Research Center (ASRC)

Introduction

The purpose of this study is to synthesize enzyme-responsive peptides for encapsulation and eventual release of the drug doxorubicin in areas of MMP-9 (cancer enzyme) overexpression. The proposed peptide sequence is FYPLGLAGRGD. Short peptides containing peptide sequence RGD can mimic integrin-binding activity of adhesive ECM, blood, and cell surface proteins. Almost half of the 20+ known integrins recognize RGD, including integrins αvβ3 and αvβ5, which are cancer-specific. By combining RGD with the MMP-9 responsive segment of our peptide, we hope to develop a peptide that targets cancer cells in areas where there is MMP-9 overexpression. Amino acid phenylalanine (F) sequences are used in peptide self-assembly to increase supramolecular interactions via aromatic contributions. Recent research has suggested that FF self-assembles into fibrils with amyloid-like deposits, suggesting an etiology for phenylketonuria (PKU). Using FY instead of FF in the proposed peptide lessens the chance of toxic fibril formation while maintaining similar fibril formation.

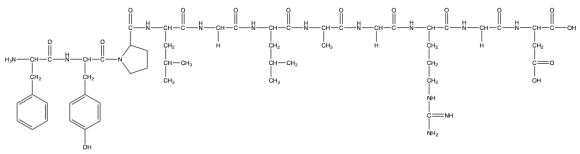

***Figure 1**: ChemDraw image of FYPLGLAGRGD peptide.*

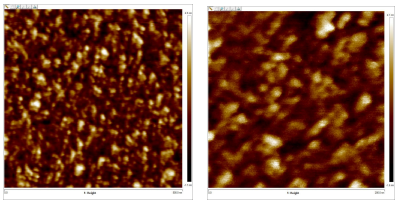

***Figure 2**: AFM images of peptide micelles.*

Materials and Methods

The peptide was prepared by solid-phase peptide synthesis (SPPS), which involved the use of Fmoc amino acids, HBTU, and N, N – Diisopropylethylamine (DIPEA) for amino acid activation; 20% piperidine in DMF was used for Fmoc deprotection. Trifluoroacetic acid (TFA) was used to release the products and the peptide was purified via lyophilization. The critical micelle concentration (CMC) of the peptide was determined by dissolving varying concentrations (0 to 1.0 mM in 0.1 increments) in deionized water. Five uL of a solution of 2 mg of pyrene in 1 mL methanol was added to each sample, mixed in order to homogenize, and the sample was transferred into a microcuvette in which the fluorescence of the resulting solution was measured by a spectrophotometer. The peptide will subsequently be cleaved by the enzyme MMP-9 in order to demonstrate drug uptake and release.

Expected Results

The peptide should self-assemble into micelles and be cleavable in areas of MMP-9 overexpression, with the purpose of improving accuracy in targeting cancer cells in the body.

MRI Compatible Polyvinyl Alcohol Cryogel Phantom to Replicate Anthropomorphic Spinal Cord Properties

Mohammad Molla [1,2,3], Vaishali Patel [2,3], Merin Grace [2,3], Robin Li [2,3], Alan C. Seifert [2,3,4], and Junqian Xu [2,3,4,5]

[1] Department of Mechanical Engineering, The City College of New York, New York, NY USA
[2] Translational and Molecular Imaging Institute, Icahn School of Medicine at Mount Sinai, New York, NY USA
[3] Department of Radiology, Icahn School of Medicine at Mount Sinai, New York, NY USA
[4] Graduate School of Biomedical Sciences, Icahn School of Medicine at Mount Sinai, New York, NY USA
[5]Department of Neuroscience, Icahn School of Medicine at Mount Sinai, New York, NY USA

An imaging phantom is needed to evaluate, analyze, and calibrate various imaging modalities in radiology such as X-Rays, MRI, CT, ultrasound, and PET. These devices often mimic and have similar properties to the native tissues of interest. Thus, such an apparatus should respond in the same manner as human tissues and organs would respond to that specific imaging modality. The human spinal cord exists in an unfavorable magnetic environment. The adjacent vertebral bodies and intervertebral discs, have different magnetic susceptibilities creating field distortions in the spinal cavity. Currently, there are no MRI compatible spinal motion phantoms that accurately capture spinal cord relaxation times, and model the spine anatomy, Cerobrospinal Fluid (CSF) flow pattern, and cord motion with respect to the cardiac cycle. We have designed a spinal phantom (Figure 1) made from polyvinyl alcohol (PVA) that features enhanced strength and MRI relaxation properties obtained through freeze-thaw cycles of an aqueous PVA solution which induces cross linking within the polymer.

The spinal cord and the subarachnoid space (SAS) between the C1 and L1 vertebral levels were modelled in SolidWorks CAD software (Dassault Systèmes, Waltham, MA) using in vivo measurements from different morphological studies. The two halves of the canal were machined using computer numerical control (HSMWorks, AutoDesk, San Rafael, CA) on two clear acrylic sheets to replicate the geometry of the SAS. A solution of 16% by weight of Polyvinyl Alcohol (PVA) 99+ %hydrolyzed (Sigma- Aldrich Inc., St. Louis, Missouri) and distilled water was made and mixed well to remove aggregates of PVA powder. The solution was autoclaved for 30 minutes at 121 degrees Celsius. The solution was weighed again and any loss of water was re-added to the autoclaved mixture. The solution was stirred continuously for 30 minutes until it reached room temperature. The solution was then transferred into 60 mL sterile syringes and injected into a 3D printed female mold using the dimensions of the spinal cord on SolidWorks. The PVA solution was allowed to settle within the mold for two hours. The mold was then subjected to one freeze-thaw cycle at -18 degrees Celsius; the mold was kept in the freezer for 17 hours and left to thaw for 48 hours before opening the mold to remove the cord. The formed 16% PVA spinal cord was stored immediately in an airtight container until phantom assembly. The denticular ligaments of the spinal cord were attached to the walls of the acrylic halves with silicone epoxy adhesive, and the two halves of the acrylic were sealed together using acrylic adhesive (Weld-On 4, SciGrip, Durham, NC). The phantom was filled with distilled water (to replicate CSF in the SAS) through a filler hole drilled on one end, and sealed with a silicone rubber stopper. The phantom was imaged using Force CT and Skyra MRI scanners (Siemens, Erlangen, Germany). Echo-planar imaging and field mapping were performed with the phantom immersed in a tub of water with three 50-mL vials (Figure 1b and Figure 1c) of air tethered to the phantom to create field distortions (Figures 2 d-f), and again without distortions (Figures 2 a-c). The relaxometry data at 3T was determined. The T_1 of the PVA spinal cord was 839 ms, and the T_2 was 107 ms. The T_1 and T_2 relaxation times in vivo of the human spinal cord are within the ranges of 700-900 ms, and 68-81 ms respectively. The concentration of PVA has a direct impact on the relaxometry data. While the T_2 time was slightly longer, adjustments to the T_2 can compromise the T_1. However, future experimentation of the ideal number of PVA freeze-thaw cycles and analysis of elongation and expansion during thawing in a controlled environment is still needed to best model the human spinal cord. A 16% by weight of PVA shows promising preliminary results. This phantom replicates normal human spinal anatomy with respect to MRI parameters. The phantom is also able to simulate field inhomogeneities because of its size allowing materials to be placed close to it. Future experiments to simulate the effects of vertebrae, respiratory, and cardiac motion within the phantom to replicate field distortions in vivo is still needed. This phantom will help facilitate technological improvements for imaging modalities in the spinal cord.

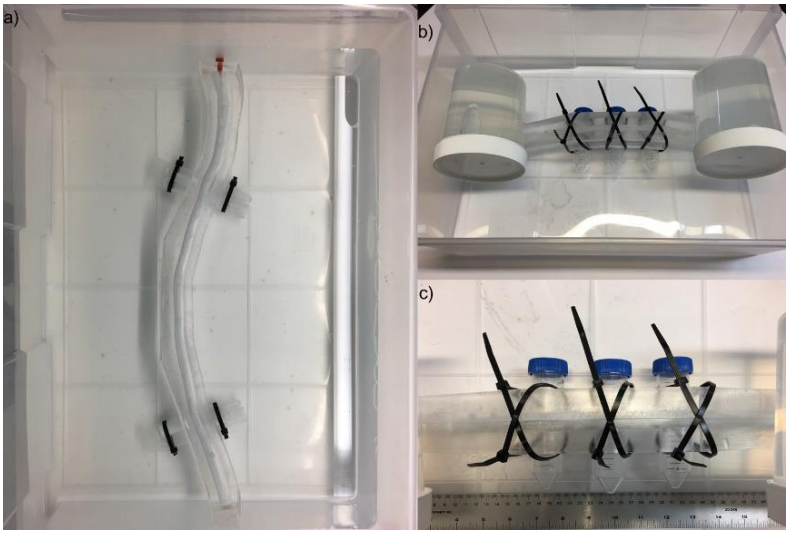

Figure 1. (a) Spinal cord phantom immersed in water (b,c) air-filled vials attached to phantom for field distortion testing

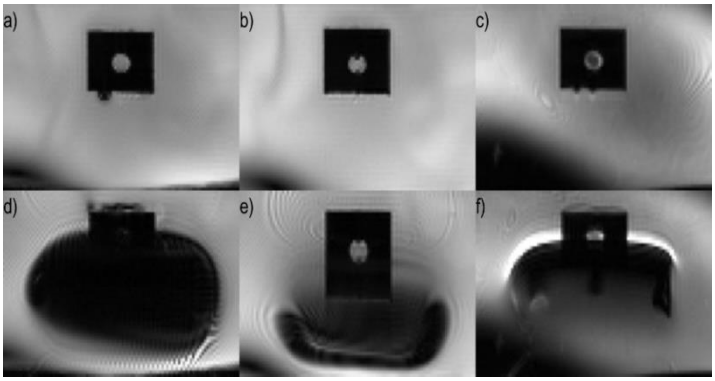

Figure 2. Echo-planar imaging sequence with typical BOLD fMRI parameters (a-c) no induced field inhomogeneities are present (d-f) field inhomogeneities produced by air-filled vials causing image distortion

Three-Dimensional Dynamics of Peptide-Polymer Hydrogel and Peptide Amphiphile Hydrogel Self-Assembly Studied Through Microrheology

Jacob Weber, Sean O'Neill, and Raymond Tu
Department of Chemical Engineering, The City College of New York, New York, NY, USA

We aim to examine the role of polymer architecture (linear and star polymers) on the dynamics of self-assembly and crosslinking through multiple particle tracking microrheology. We bioconjugate PEG-based polymer end groups with coiled-coil forming polypeptides, and compare the rates of self-assembly as a function of the concentration and type of peptide-conjugated PEGs in solution. When placed in salt solution, the polypeptides fold into the proper secondary structure to initiate the liquid-solid transition into a hydrogel.

Additionally, we aim to examine the time dependent pH responsiveness of a peptide amphiphile on the dynamics of self-assembly and cross-linking through microrheology. We conjugate a palmitic acid end group to a beta-sheet forming peptide amphiphile, and compare the rates of self-assembly as a function of concentration and pH. The evolution of secondary structure with polymer self-assembly is measured using circular dichroism, and the evolution of fibrillar assemblies is measured as a function of amphiphile concentration using multi-angle light scattering.

Fluorescent microbeads are used as tracking particles for multiple particle tracking microrheology, which is used to measure the material properties of the polypeptide solution as it makes the liquid-solid transition. The weighted centroid method is used for particle tracking, and the ensemble-averaged mean-squared displacement is calculated. Master curves are generated, and shift factors are plotted versus time, allowing the critical gel exponent and critical gel time to be determined.

SM50 and calcium carbonate crystals nucleation

Martin Pendola[1], Gaurav Jain[1], John Spencer Evans[1]
(1)Laboratory for Chemical Physics, New York University Center for Skeletal and Craniofacial Medicine, 345 E. 24th Street, NY, 10010 USA

INTRODUCTION:
SM50 is ~50 kDa protein, part of a subfamily of C-type lectin-like domains, and it plays a role in the mineralization of sea urchin embryo spicule (Mann et al 2010). The sea urchin spicule is a mineralized structure based on calcite, with only a 1% of organic matrix, which includes SM50 protein traces.(Seto et al 2004). However, the understanding of SM50 function in the mineralization of sea urchin spicule is far from complete.

MATERIALS AND METHODS:
A chemically synthesized version of SM50 was dissolved in unbuffered distilled water and used to run mineralization assays (SM50 1.5uM, CaCl 100mM, pH 8.1) on a silicon wafer. SEM imaging of the precipitated crystals and TEM of the supernatant solution was also performed. Subsequently, we carried a flow cytometry analysis of SM50 solutions and AFM imaging in the same conditions, to evaluate the aggregation properties of the protein. MALDI-TOF experiments (1.5uM concentration, 2.6 DHA matrix) was conducted to evaluate the oligomerization of the protein.

RESULTS;
SM50 shows strong aggregation properties. Flow cytometry and AFM show the strongest aggregation is produced in presence of Ca++. MALDI TOF suggests SM50 is prone to oligomerization, but the m/z peaks are not possible to resolve using MALDI. TEM images show elongated nucleation sites inside the protein hydrogel, consistent with the results observed in other proteins of the same subfamily. SEM shows SM50 produced a nano-scale modification in the calcium carbonate crystals and nucleation of calcite polymorphs, which proved to be laterite using electron diffraction analysis. Focused Ion Beam Tomography discovered the presence of micro-cavities inside the crystals. EDS showed a different Calcium ratio for SM50 positive crystals.

CONCLUSIONS:
SM50 favors the formation of protein hydrogel-like clusters, where calcium carbonate nucleation occurs. The presence of nano-scale porosities and surface modifications, which has been observed previously (Chang et al 2015), seems to be a consequence of the nucleation inside the SM50 gel-like protein aggregates.

MARTINI Coarse Grained Studies of Aggregation Behaviors of Ultrashort Peptide Mixtures

Srinivas Mushnoori[1] and Meenakshi Dutt[1]

[1]*Department of Chemical and Biochemical Engineering, Rutgers, The State University of New Jersey, Piscataway, NJ-08854*

ABSTRACT

Peptide-based materials is an area that has seen a surge in interest recently due to its wide range of potential applications including targeted drug delivery, cancer treatment, tissue engineering, treatment of neurodegenerative diseases, nanoelectronics and antimicrobial surfaces. In this project, a coarse-grained model is employed in conjunction with Molecular Dynamics simulations to study the structure and dynamical processes underlying the aggregation behavior of a wide range of di- and tripeptides. The self-assembly of these molecules into various ordered nanostructures such as vesicles, nanotubes, nanorods and micelles, and disordered structures such as hydrogels is explored. Specifically, mixed peptide systems are considered and the effect of their relative concentrations is investigated.

Boronization of Dental Implants

Gabriel Kaye[1], Jonathan Morcos[1], Michelle Bowers[1], Vishnu Reddy[1], Lukasz Witek[1], Nick Tovar[1], Roumiana S. Petrova, Paulo Coelho[1,2]

[1]Department of Biomaterials & Biomimetics, NYU College of Dentistry
[2]Hansjorg Wyss Department of Plastic Surgery, NYU Langone Medical Center

Purpose: Titanium implants have shown the ability to facilitate osseointegration and therefore are used to achieve long-term anchorage between bone and implant (1). However, early implant failure rates have been reported at ~6% (2). Implant surface treatments have been employed in an effort to minimize this risk by altering the surface roughness and chemistry to induce greater osseointegration. Previous studies have shown that boron has the ability to facilitate odontogenic and osteogenic differentiation and to accelerate proliferation of osteoblast-like cells on titanium surfaces, but never in a dental model (3)(4). The aim of the study was to explore the application of elemental boron on titanium dental implants and its effect on osseointegration.

Methods: Forty implants were surgically placed into the iliac crest of 10 male sheep, four in each sheep. There were four groups of implants; as machined untreated titanium implants, boronized implants, acid-etched implants, and acid-etched boronized implants. The concentration of boron in Titanium diboride was 14wt%. The animals were sacrificed at 3 and 6 weeks and the implants were processed for histologic assessment. Osseointegration and bone growth were determined by calculating the percentage of bone in contact with the implant (BIC) and percentage of bone within in the healing chambers (BAFO) (5).

Results: The untreated machined implants showed a 19.9% BAFO at three weeks, which significantly increased to 33.8% BAFO at six weeks. The acid-etched implants had a BIC and BAFO of 33% and ~31% respectively at three weeks and with an increase in BIC to 37% and significantly increased BAFO to 46.2% by six weeks ($p=0.277$ and $p=0.441$ for BIC and BAFO respectively). Alternatively, the boronized and acid-etched boronized had lower BIC and BAFO than their respective controls. The boronized samples had a BIC and BAFO of 16.4% and 27.3% respectively at three weeks, which significantly decreased to 9% and 18.5% respectively at six weeks ($p<0.001$ for BIC and BAFO). The acid-etched boronized implants had a BIC and BAFO of 21.7% and 25.9% respectively at three weeks and which significantly decreased to 5.9% and 17% at six weeks ($p<0.001$ for BIC and BAFO).

Conclusions: Histological analysis showed that boronization of the implant surface caused bone demineralization. Comparing the three week and six week time points showed receding hard tissues and by six weeks, hard tissue had regressed to demineralized osteoid tissue. Interestingly, the demineralization of bone only occurred with new woven bone and no demineralization was seen in older lamellar bone. This effect was only seen in the boronized samples, and was even more apparent in acid-etched boronized implants, and not in the control groups, which had an increase in bone growth over time. Localized boron surface treatment is potentially supra-physiologic, thereby causing a decline in osseointegration.

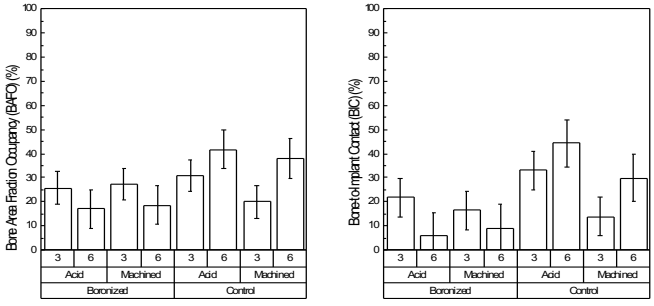

References

1. Albrektsson, T., Brånemark, P. I., Hansson, H. A., Lindström, J. Osseointegrated titanium implants: requirements for ensuring a long-lasting, direct bone-to-implant anchorage in man. *Acta Orthopaedica Scandinavica* 1981;52:155-170.
2. Olmedo-Gaya, M. V., Manzano-Moreno, F. J., Cañaveral-Cavero, E., de Dios Luna-del Castillo, J., Vallecillo-Capilla, M. Risk factors associated with early implant failure: A 5-year retrospective clinical study. *The Journal of prosthetic dentistry* 2016;115:150-155.
3. Tasli, P. N., Dogan, A., Demirci, S., Sahin, F. Boron enhances odontogenic and osteogenic differentiation of human tooth germ stem cells (hTGSCs) in vitro. *Biological trace element research* 2013;153:419-427
4. Huang, Q., Elkhooly, T. A., Liu, X., et al. SaOS-2 cell response to macroporous boron-incorporated TiO 2 coating prepared by micro-arc oxidation on titanium. *Materials Science and Engineering: C* 2016;67:195-204
5. Leonard, G., Coelho, P., Polyzois, I., Stassen, L. and Claffey, N. (2009), A study of the bone healing kinetics of plateau versus screw root design titanium dental implants. Clinical Oral Implants Research, 20: 232–239. doi:10.1111/j.1600-0501.2008.01640.x

Trabecular metal [TM] and tapered-screw vent [TSV] with Osseodensification in low-density bone

Gregory Kurgansky[1], Adham Alifarag[1], Christopher Lopez[1,2], Lukasz Witek[1], Nick Tovar[1], Paulo Coelho[1]

[1] Department of Biomaterials and Biomimetics, New York University College of Dentistry
433 1st Avenue Room 862
New York, NY 10010
[2] Icahn School of Medicine at Mount Sinai
1 Gustave L. Levy Pl,
New York, NY 10029

Purpose: Surgical fixation of implants into bone for the correction of bone deformities or defects is a traditional approach for skeletal stabilization. Important measures of efficacy of implants include implant stability and osseointegration—the direct interaction between living bone and an implant. [1] These include primary stability, which is the initial tight interlocking between bone and implant immediately after fixation, and secondary stability that encompasses bone regeneration and remodeling around the implant. Although there have been numerous studies and improvements in the fixation of hardware, the ongoing fixation failures in bone implants have established the necessity for enhancements in hardware, design, and surgical instrumentation.[2] A new method called Osseodensification (OD) utilizes a drilling technique that induces compaction of the osteotomy wall and leads to greater bone-implant contact and primary stability. The objective of this study was to identify the histologic and mechanical effects of osseodensification, through the use of two different implants.

Methods: Six implants were installed in the ilia of six male sheep (n=6) bilaterally, with each implant measuring 3.7mm in diameter x 10mm length. Two sheep had implants installed with the traditional subtractive drilling meanwhile four sheep had implants installed with osseodensification. Three of the six implants on each side of the ilia were trabecular metal (TM) and three were tapered-screw vent (TSV). In order to measure primary stability, the insertion torque of all implants was recorded by a digital torque meter (Tonichi STC2-G, Tonishi, Japan). A three-week period post-surgery was given to allow for healing to take place after which all six sheep were euthanized and the ilia were collected. After retrieval, the bone-implant blocks were dehydrated in progressing ethanol solutions, embedded in methyl methacrylate-based resin, and cut using a diamond saw (Isomet 2000, Buehler Ltd., Lake Bluff, IL, USA). The prepared slides were stained in Stevenel's blue and Van Geison to distinguish bone, and the soft and connective tissues. In order to determine the osteogenic values surrounding the surface of the implant, Bone-implant contact (BIC) and bone area fraction occupancy (BAFO) were quantified.[3] All statistical analyses were completed with IBM SPSS (v23, IBM Corp., Armonk, NY).

Results: Mechanical testing delineated significantly higher levels of insertion torque for the OD (~70 N cm) group relative to the Regular (R) (~47 N cm) group (p<0.05). Furthermore, when comparing TSV to TM implants, there were significant differences between insertion and removal torques (58 and 84 Ncm, respectively) of the TSV, regular drilling group. (Figure 1) This is attributed to the fact that the presence of threads, such as in TSV, improves the mechanical interlocking of the implant with the osteotomy. Histomorphometric analysis showed that statistical differences were present between OD (%BIC ~50) and R (%BIC ~40) (p= 0.037). For histological analysis, even though all samples demonstrated degrees of osseointegration, the methods using Densah burr and osseodensification, (OD) both showed considerably greater degrees of osseointegration when compared to the R group.

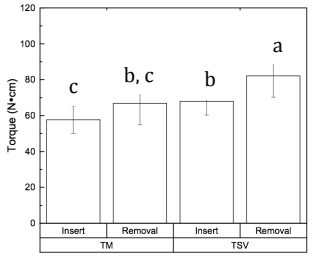

Figure 1: Comparison of Insertion and Removal Torques in TM vs. TSV Implants

Conclusion: The utilization of OD as a design for improved fixation of hardware was supported by increased levels of stability, both primary and secondary. Mechanical and histological data with OD provided notably different results from those of the regular drilling method. Overall, OD instrumentation had greater stability and the TSV implant demonstrated superior interlocking due to an increased amount of threads. Osseodensification merits further assessment in other surgical contexts.

References

1. Christopher D. Lopez Adham M. Alifarag, Andrea Torroni, Nick Tovar, J. Rodrigo Diaz-Siso, Lukasz Witek, Eduardo D. Rodriguez, Paulo G. Coelho, Osseodensification for enhancement of spinal surgical hardware fixation. *Elsevier 12 January 2017*

2. Levin L. DEALING WITH DENTAL IMPLANT FAILURES. Journal of Applied Oral Science. 2008;16(3):171-175.

3. SOARES, Priscilla Barbosa Ferreira et al. Influence of Implant Surfaces on Osseointegration: A Histomorphometric and Implant Stability Study in Rabbits. *Braz. Dent. J.* [online]. 2015, vol.26, n.5 pp.451-457

Synthesis of a 3D-Patterned Fetal Trachea Construct Mimicking the Mechanics of the Native Fetal Trachea

Elizabeth G. Mansfield (1), **Jamie M. Benson (1)**, Debra T. Auguste (2)

1. Department of Biomedical Engineering, CUNY City College of New York, New York, NY
2. Department of Chemical Engineering, Northeastern University, Boston, MA

Introduction:

Obstructions or congenital defects in the trachea that impede respiration are almost always fatal. The many attempts to surmount this issue, including surgical techniques and natural and artificial prosthesis have been resulted in inconsistent outcomes. Increasingly, focus has turned to tissue engineering and the use of biomaterials to develop tracheal constructs. For full functionality, an engineered replacement likely must mimic native tissue mechanical properties. We have synthesized a 3D, patterned, fetal tracheal construct comprised of a methyl acrylate methyl methacrylate copolymer (MA-co-MMA). Hard and soft segments, with a 1:2 hard to soft ratio, and a soft vertical region were patterned within the construct to mimic the native tracheal architecture of horseshoe shaped cartilaginous rings connected by ligament, and bridged by trachealis muscle. Hard regions have a modulus within the range of tracheal cartilage, and soft segments within the range of trachealis muscle.

Methods:

MA-co-MMA polymer tubular constructs were synthesized in custom molds and patterned through 3D UV-photolithography in an RMR-600 Photochemical Reactor. Compliance testing was performed in a closed system, heated water bath to create changes in pressure, in terms of cmH_2O. Longitudinal tensile testing was performed on the hard and soft segments using an Instron mechanical testing system.

Results:

MA-co-MMA tubular constructs were synthesized and characterized with a 1:2 hard: soft ring size with hard and soft rings within the range of native tracheal cartilage and annular ligament. This ring size ratio was shown previously[1] to provide closely matched longitudinal and radial properties. We identified UV-photopolymerization times to obtain the desired MA-co-MMA moduli for hard and soft regions. Subsequently we evaluated two different tubular geometries – one with uniform tube wall thickness, and one with a gradually reducing wall thickness reducing towards the soft vertical region. The nonuniform tube wall thickness resulted in construct collapsing compliance within the published range for native trachea, as shown in Figure 1. Constructs were additionally evaluated for longitudinal mechanical properties and yield behavior. Normal tracheal extension during respiration will occur within the elastic range of the synthesized constructs.

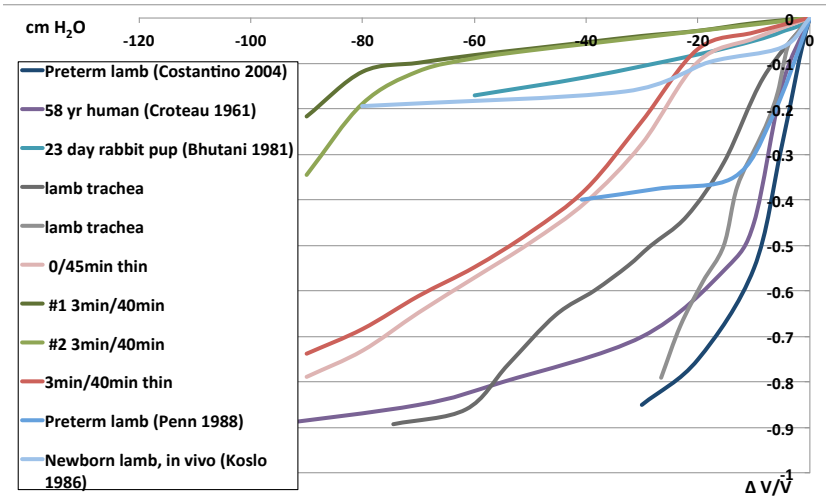

Figure 1: Compliance in published studies compared to our measurements of construct and sheep trachea compliance.

Discussion and Conclusions:

The toughness and longitudinal extensibility of the trachea are of great importance for the efficient passage of air within the body. Mismatched mechanical properties of an implant may lead to fatal obstruction or bleeding[2], and proper compliance is required for effective coughing which reduces risk for infection[3]. While modulus matching of the biomaterial to the native tissue is of necessity, the geometry of the tubular construct also plays an integral role in achieving proper organ level mechanics. We found that a nonuniform wall thickness of the construct allows for a compliance that more closely matches that of the native trachea. We produced a 3D, biomimetic tracheal construct with compliance and longitudinal mechanical properties that are within the range of the fetal trachea.

References:

(1) Mansfield EG *et al.* Acta Biomat 33 176-82, 2016. (2) Kawaguchi, S *et al*. Biomaterials, 2001. 22(23):p. 3085-90; (3) Malve M *et al.* J Biomech Eng 2011;133:021001

Modulation of collagen fibrillogenesis using ammonia gas to vary optical characteristics and biological compatibility of biosynthetic corneal implants.

Shoumyo Majumdar(1), Xiaokun Wang(1), Anirudha Singh(1), Oliver Schein(3), Jennifer Elisseeff(1,2)
(1) Translational Tissue Engineering Center, Johns Hopkins School of Medicine, Baltimore, MD
(2) Wilmer Eye Institute, Johns Hopkins School of Medicine, Baltimore, MD

Purpose

Factors such as pH, temperature and ionic strength help modulate collagen fibril formation. Our lab has previously developed type I collagen based 'vitrigel' biomaterial via a controlled collagen self-assembly process. In our current study, we aim to influence fibrillogenesis in 'vitrigel' biomaterials through alternative gelation techniques using ammonia gas permeation, and assess the role of fibrillar networks in optical and biological properties and performance in vivo.

Methods

Ammonia-Mediated Collagen (AMC) gelation was achieved through exposure of 5mg/ml bovine collagen to ammonia vapors for different durations, gelation at 37°C, followed by slow vitrification at 5°C for 1 day and 40°C for 1 week and rehydration in buffer. Materials were tested for transparency in the visible spectrum, and fibrillogenesis was visualized using SHG microscopy. In vitro biocompatibility was tested using primary rabbit epithelial cells, followed by in vivo implantation in rabbit model.

Results

AMC vitrigels were prepared at physiologically relevant thicknesses, with varying transparencies as measured using a microplate reader. The transparency of the vitrigels corresponded to degree of fibrillogenesis. This was observed using Second Harmonic Generation microscopy (Figure 1).

Additionally, material biocompatibility was verified through *in vitro* proliferation studies and subsequent immunostaining for key epithelial cell markers. Further, *in vivo* implantation using interrupted sutures in a pilot rabbit study demonstrated stability and viability of the AMC vitrigel corneal implant material (Figure 2).

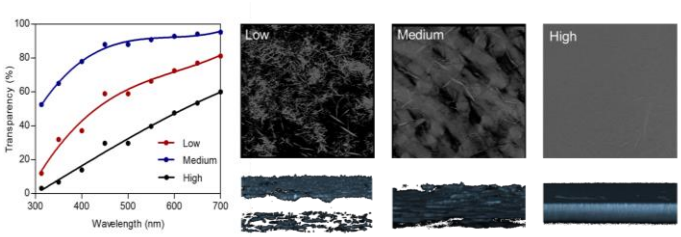

Figure 1: Transparency of AMC membranes over visible light spectrum corresponds to degree of collagen fibrillogenesis with low, medium and high ammonia exposure times.

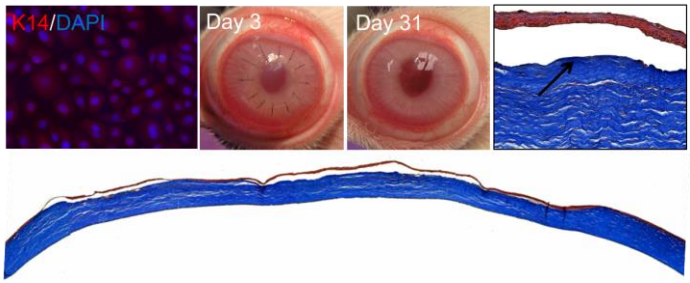

Figure 2: AMC vitrigels demonstrate in vitro biocompatibility and stain for K14 epithelial marker. AMC implanted in rabbit using interrupted sutures show full reepithelialization and integration with host cornea by day 31.

Conclusions

The production of AMC vitrigels through varying degrees of exposure to ammonia demonstrates that the collagen ultrastructure of vitrigels is tunable. Further, bulk material properties such as transparency can be modulated by changing the underlying ultrastructure achieved through the versatility of the gelation process involving ammonia exposure. AMC materials also demonstrate the cytocompatibility through *in vitro* studies. In addition suturability, biocompatibility and integration with host cornea *in vivo* was also demonstrated, indicating a viable option for a biosynthetic cornea.

Efosa Amadasu, Rebecca Romero Aburto, Konstantin Sokolov
The University of Texas MD Anderson Cancer Center

Scale Up Synthesis of Iron Oxide for Magnetic Relaxometry

Abstract

Introduction:
A recent method for molecular imaging, Magnetic Resonance Relaxometry (MRX) has been found to measure the magnetization of nanoparticles. First a short-lived DC magnetic pulse is applied to the nanoparticles aligning their magnetic moments. The pulse is turned off and the decay or relaxation of the magnetic moments are detected by Superconducting Quantum Interface Device (SQUID) detectors which can detect fields of the order of picoTesla. Magnetite (Fe3O4) or iron oxide is the choice of nanoparticle used for MRX. Superparamagnetic iron oxide nanoparticles (SPIONS) are also non-toxic in the body relative to other contrasting agents such gadolinium and radioactive tracers.

The sensitivity of magnetic relaxometry can be increased by increasing the amount of nanoparticles attached to cells up until a saturation point where all the cells are bound to nanoparticles. The research question asked was how to scale up the quantity of iron oxide particles per batch while keeping the hydrodynamic size below 100 nm and polydispersity below 0.3?

Hypothesis:
By changing the lipid excess factor, PEG molecular weight, and stirring speed of the hot plate used in the reaction, the iron oxide micelles can be scaled up from 240 uL (72 ug)/batch to 600 uL (180 ug)/batch and 1500 uL (450 ug)/batch.

Methods:
Iron oxide micelles were synthesized by flow synthesis oil in water microemulsion and centrifuged to remove aggregates, empty micelles, and water.

Results/Conclusion:
The hydrodynamic size of the purified micelles were measured by dynamic light scattering. The results showed decreasing the molecular weight of PEG decreases the hydrodynamic size of the resulting micelles. Also changing the lipid excess factor from 10% to 30% to 40% decreased the z-averaged hydrodynamic size of the iron oxide micelles. The size of iron oxide micelles had no correlation with the stirring speed of the magnetic stirrer. Future work for the successfully scaled up iron oxide micelles involves in vivo superparamagnetic relaxometry (SPMR) and in-vitro macrophage studies.

Optimizing Bovine Corneal Decellularization Procedure for Corneal Substitute

Yu Jung Shin[1], J Jeremy Chae[2], Jennifer Elisseeff[1,2]

[1]Department of Biomedical Engineering, Johns Hopkins University, Baltimore, Maryland
[2] Wilmer Eye Institute, Johns Hopkins University, Baltimore, Maryland

Purpose: In previous studies, we have shown that the reconstructed decellularized porcine cornea is capable of corneal tissue regeneration. However, the size limitation of porcine cornea prevents a complete coverage of human cornea. Additionally, porcine tissues are prohibited in certain cultures. In order to address these issues, we have optimized a decellularization process specific to the bovine cornea. The purpose of this study is to optimize a non-immunogenic tissue based material which can be reconstructed into highly transparent corneal substitute.

Methods: Native bovine corneal tissues were dissected from fresh bovine eyes and washed in anti-bacterial and antifungal solutions. Afterwards, decellularization procedure was performed with 1% sodium dodecyl sulfate treatment (24hrs) followed by 1% Triton-X treatment (24hrs, 48hrs, 72hrs). Each set of cornea (N=5) was immersed in same amount of solutions and incubated under the same stirring speed (150rpm) to ensure identical diffusion and shear stress. Efficiency of decellularization method was assessed by Hochester dye (1ug/ml in TNE buffer) DNA quantification with fluorometer. Qualitative analysis of decellularization was conducted using H&E staining. Statistical analysis was performed by two tailed student's t test and the data was presented with mean ± standard deviation.

Results: DNA content of decellularized cornea was significantly reduced at all 48hr, 72hr, and 96hr time points ($p=0.000$) compared to that of native cornea (2.969±0.086 µg/mg). The lowest mean DNA content was observed after 72 hours of SDS-Triton-x treatment (0.296±0.026 µg/mg) compared to mean DNA contents after 48 hours (0.391±0.027 µg/mg) and 96 hours (0.394±0.106 µg/mg) of treatment. Student's t test showed a significant decrease in DNA content between 48hr and 72hr time points ($p=0.001$). However, no significant difference was measured between 72hr and 96hr time points ($p=0.142$). The efficiency of 72hr SDS-Triton-x treatment was further supported by H&E staining. The 72hr sample did not show any hematoxylin staining, suggesting effective removal of cells.

Conclusion: Efficiency of decellularization is crucial in engineering a non-immunogenic material. Our results show that we have successfully optimized the decellularization condition for bovine corneal tissues. Through further vitrification and molding process, we aim to optimize a reconstructed decellularized bovine cornea with enhanced functions.

MEASURING THE NANOMECHANICAL PROPERTIES OF TOMATO CUTICLES USING ATOMIC FORCE MICROSCOPY

Stephan O. Smith (1), Keyvan Dastmalchi (2), and Ruth E. Stark (3)

Department of Chemistry and Biochemistry, City College of New York, New York, NY, 10031

Tomato plants (*Solanum lycopersicum)* possess an outer skin surface called the cuticle. The cuticle has two components: a mixture of waxes and the cutin polymer. Tomato fruit is subjected to stresses from biotic, environmental, and mechanical factors, leading to decreased crop yield and economic losses. It is important to understand the relationship between the chemical composition and the biomechanical properties of tomatoes. This project assesses the influence of cutin deposition on the nanomechanical properties of the tomato cuticle using Atomic Force Microscopy (AFM). The resistance to deformation (Young's moduli) of the glossy surface of dewaxed and waxy tomato outer cuticles from wild type (M82) and two RNAi-silenced cultivars (deficient in cutin synthase enzymes CUS1 and CUS2) were compared under controlled humidity (60%). For dewaxed samples a downward trend in Young's modulus (M82, CUS2 and CUS1) was observed for the glossy surface, indicating that the elasticity of tomato cuticle is positively correlated to the amount of cutin deposition within the sample. For the corresponding waxy samples, however, CUS1 and CUS2 displayed a higher Young's modulus than M82. It was concluded that in the absence of epicuticular waxes, cutin deficiency in CUS1 and CUS2 contributes to a lower resistance to deformation and decreased stiffness of the cuticles. However, for the waxy samples the scenario is quite the opposite; the higher Young's modulus values for CUS2 and CUS1 can be attributed to higher wax-to-cutin ratios in the CUS-silenced cuticles. Future work will correlate these results with macroscale force-to-failure measurements and molecular characterization by solid-state NMR and mass spectroscopy, to better understand the underlying changes in physical and chemical composition that produce cultivar-specific differences in nanomechanical performance.

Mechanical Evolution of alpha-helical peptide linear and star Poly-ethylene

*Sean C. O'Neill and Raymond S. Tu**

Department of Chemical Engineering, The City College of City University of New York, 140th Street and Convent Avenue, Steinman Hall T313, New York, New York 10031

ABSTRACT: We have sought to examine intra-/inter-molecular dynamics of peptide gelation via design of a peptide conjugated poly-ethylene glycol (PEG) system, that allows us to investigate the dynamics of self-assembly. Through a bottom-up approach, we have designed a synthetic 23-amino acid peptide sequence by Fmoc-Solid Phase Peptide Synthesis (SPPS), followed by Circular Dichroism (CD) Spectroscopy in order to demonstrate that the peptide conjugates fold into an α-helical configuration with increasing electrolyte concentrations. Furthermore, upon a change in secondary structure the peptide sequence forms coiled-coil helical self-assemblies, which can be inter- or intramolecular coiled-coils. These peptides were tethered to distinct PEG architectures, end-functionalized linear- and star geometries. Under the appropriate conditions, we hypothesize that infinite cross-linked self-assembled structures will result as intermolecular self-assembly dominates the coiled-coil structure formation. By applying microrheology and principles of percolation theory, we can investigate this hypothesis by measuring kinetics of gelation for linear and star peptide-PEG bioconjugates and correlate the gelation behavior with the molecular structure and self-association. While we fully expected the star-PEG conjugates to yield stronger faster forming gels, this study shows that the dynamics of peptide folding and assembly for linear-PEG conjugated systems yield a percolated network, but the star-PEG conjugated systems yield discrete assemblies and remain viscous. These results suggest that the degree of intra- and inter-molecular folding defines the critical gel behavior of the supramolecular system.

Peptide—PEG—Peptide

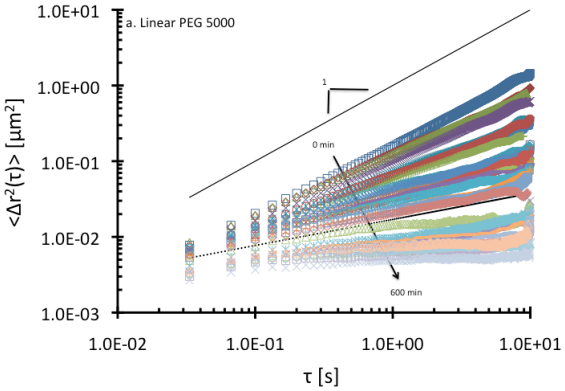

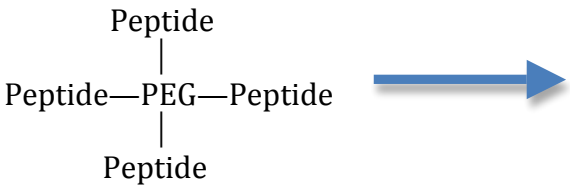

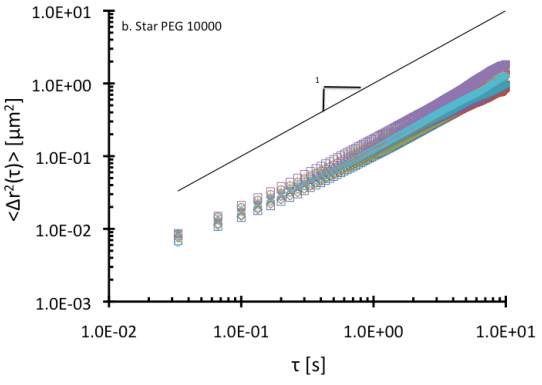

Comparison of Graft Fillers with Membranes Using *in vivo* Model

Madison Cox(1), Lukasz Witek(2), Karen Song(3), Jeremy Mao(3), Paulo Coelho(2)

1. Department of Biomedical Engineering, Columbia University, New York, NY, USA
2. Department of Biomaterials and Biomimetics, New York University, New York, NY, USA
3. Center for Craniofacial Regeneration (CCR), Columbia University Medical Center, New York, NY, USA

Introduction – Dental grafts and membranes are often used together due to the widely held assumption that membrane inclusion is necessary to keep soft tissue from growing into the bone cavity.[1, 2] However, it is unclear the effect a barrier membrane has when used in combination with specific grafts. Additionally, complications can occur due to the graft itself, thus leading to infection, partial and total graft loss, and dehiscence.[3] This study aimed to examine the effect of the barrier membrane used in conjunction with an SBC and Vivoss (Straumann®, Basel, Switzerland) graft. The grafts with and without a membrane were then compared.

Methods – These grafts were surgically embedded into Beagle dogs and then removed after 8 weeks. After preparing the samples through cutting, polishing, staining, and scanning, 2D histology was used to determine the percentage of bone, soft tissue, and dental graft for these five trials.

	Average Bone Percentage (%)	Average Graft Percentage (%)	Average Tissue Percentage (%)
Vivoss and Membrane	78.813	3.0079	18.179
Vivoss	70.159	11.426	18.415
SBC and Membrane	60.312	10.125	29.564
SBC	64.111	9.0865	26.803

Table 1: **Area percentages of bone, graft, and soft tissue**

Results – The Vivoss graft without a membrane had an average bone area less than the Vivoss graft with a membrane (table 1). Additionally, it had more tissue in the cavity, but the averages are similar. In contrast, the SBC graft without a membrane showed more bone growth and less soft tissue than the SBC graft with a membrane had. When comparing the grafts, the Vivoss graft had more bone area and less soft tissue than the SBC graft.

Discussion – Membranous barriers are intended to limit soft tissue infiltration, but the experimental membrane seemed to have limited success. The control had the most bone area while also having the least amount of soft tissue and graft. The Vivoss graft with and without a membrane performed better than the SBC graft with and without a membrane, suggesting the Vivoss graft is more effective. While the Vivoss graft with a membrane had more bone growth than only the Vivoss graft, the cause could be unrelated to the membrane since the average soft tissue in each is similar.

References:

1. Schenk, R.K., Buser, D., Hardwick, W.R., Dahlin, C. (1994) Healing pattern of bone regeneration in membrane-protected defects: a histologic study in the canine mandible. *International Journal of Oral and Maxillofacial Implants* 9: 13-29

2. Sculean A, Nikolidakis D, Schwarz F. (2008) Regeneration of periodontal tissues: combinations of barrier membranes and grafting materials - biological foundation and preclinical evidence: a systematic review. *J Clin Periodontol*. 2008; 35(8 Suppl):106–16.

3. Deluiz D., Oliverira L., Fletcher P., Pires F., Nunes M., Tinoco E. (2016) Fresh-Frozen Bone Allografts in Maxillary Alveolar Augmentation: Analysis of Complications, Adverse Outcomes, and Implant Survival. *Journal of Periodontology* 87: 11: 1261-67

Quantifying Bone Regeneration in 2 Dimensions vs. 3 Dimensions is Equal in a Long Bone Model

Rosen Jeong(1), Lukasz Witek(1), Pablo Atria(1), Nick Tover(1), Paulo Coelho(1, 2)
1. Department of Biomaterials and Biomimetics, New York University College of Dentistry, New York, NY, USA
2. Hansjörg Wyss Department of Plastic Surgery, New York University School of Medicine, New York, NY, USA

I. INTRODUCTION

This study focuses on *in vivo* studies conducted in a preclinical animal model, involving the development and subsequent analysis of bone substitute materials. A majority of analyses on the healing kinetics of these grafting materials are done on calcified histological, two-dimensional (2D) sections[1,2]. However, micro-computed tomography (μCT) rendered analysis has garnered much attention in the bone tissue engineering field. In this study, quantification and analysis of post-operative bone and grafting material μCT images, reconstructed with 3-dimensional software, is compared to traditional 2D histomorphometry. This study utilized two previous *in vivo* studies, with defects created and filled with grafting materials, in the (1) dog mandible and (2) rabbit radius. Dissimilar to previous publications that compare 2D and 3D techniques qualitatively[3,4], this study assesses the correlation between the two imaging modalities.

II. METHODS

Group 1 received a granular bioactive ceramic in the defect, while group 2 received a bioactive 3D printed scaffold in the defect. As this was a study of quantification technique, time *in vivo* was not considered. Prior to and during μCT scanning, the samples were stored in 70% ethanol. Each sample was scanned using μCT Scanco 40 (Scanco Medical, AG, Basserdorf, Switzerland). Raw μCT digital imaging and communications in medicine (DICOM) data was analyzed using Amira® software (VSG, Burlington, MA)[5]. Each image file was segmented manually using a volume-editing tool, and the scaffold was isolated from the surrounding structures; individual sections were examined, and bone and scaffold were differentiated from each other. This permitted acquisition of a specific color-coded image of each sample, and the quantification of the volume, by software, of both materials via material statistics tool based on voxel quantity[5,6]. After μCT scanning, samples were prepared for calcified histological processing, and then embedded using a methacrylate-based resin (Technovit 9100, Heraeus Kulzer GmbH, Wehrheim, Germany)[6-8]. The polymerized samples were then cut, glued to acrylic plates, subjected to grinding, and polished. A Stevenel's Blue and Van Giesons Picro Fuschin differential tissue staining protocol was used for the sections, which were then scanned to digital format using a histology slide scanning system. The image was then color-coded via Photoshop software (Adobe, San Jose, USA), and an image thresholding software was then used to quantify percentage values based on specified colors with precise results of megapixel accuracy[6-8].

III. RESULTS

No significant differences between 2D histomorphometry and 3D μCT Amira analysis methods were observed.

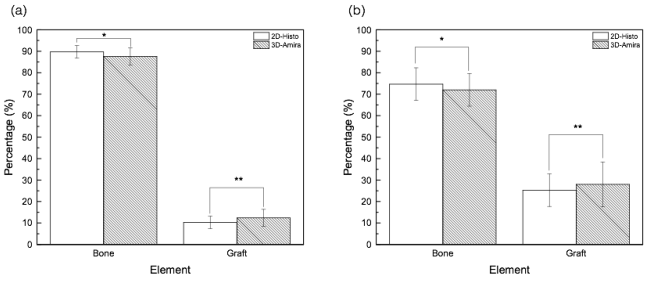

Figure 1: Box plots with 95% confidence intervals of both experimental groups (a) Granular, and (b) scaffold techniques. The asterisks represent statistically homogenous groups.

IV. DISCUSSION

The results suggest that quantification by either 2D histomorphometry or 3D μCT Amira analysis can be used independently. Comparison of data suggests that there is no significant difference between outcomes of the two techniques. However, differences do exist. Microscopic histomorphometry (2D) analysis prevents further studies on samples as they are *'destroyed'* during processing. Alternatively, 3D analysis is a nondestructive investigatory tool that permits three-dimensional bone structure reconstruction, and a visual representation of the defect in terms of volume. A shortcoming of 3D analysis is user dependence- variability in image analysis often varies more than 2D analysis. This suggests that with high resolution μCT scans and single-user operation, quantification via μCT and subsequent Amira analysis is a suitable alternative to histomorphometry.

REFERENCES

[1] Jensen SS, Yeo A, Dard M, Hunziker E, Schenk R, Buser D. Evaluation of a novel biphasic calcium phosphate in standardized bone defects. A histologic and histomorphometric study in the mandibles of minipigs. Clinical oral implants research. 2007;18:752-60.
[2] Jensen SS, Bornstein MM, Dard M, Bosshardt DD, Buser D. Comparative study of biphasic calcium phosphates with different HA/TCP ratios in mandibular bone defects. A long-term histomorphometric study in minipigs. Journal of Biomedical Materials Research Part B: Applied Biomaterials. 2009;90:171-81.
[3] Davis GR, Fearne JM, Sabel N, Norén JG. Microscopic study of dental hard tissues in primary teeth with Dentinogenesis Imperfecta Type II: Correlation of 3D imaging using X-ray microtomography and polarising microscopy. Archives of oral biology. 2015;60:1013-20.
[4] Freitas GP, Lopes HB, Martins-Neto EC, de Almeida AL, de Oliveira PT, Beloti MM, et al. Effect of Nanotopography Created by H2SO4/H2O2 on Bone Response to Titanium Implant. Journal of Oral Implantology. 2015.
[5] Vandeweghe S, Leconte C, Ono D, Coelho PG, Jimbo R. Comparison of histological and three-dimensional characteristics of porous titanium granules and deproteinized bovine particulate grafts used for sinus floor augmentation in humans: a pilot study. Implant Dentistry. 2013;22:339-43.
[6] Tovar N, Jimbo R, Gangolli R, Perez L, Manne L, Yoo D, et al. Evaluation of bone response to various anorganic bovine bone xenografts: an experimental calvaria defect study. International journal of oral and maxillofacial surgery. 2014;43:251-60.
[7] Tovar N, Jimbo R, Gangolli R, Witek L, Lorenzoni F, Marin C, et al. Modification of xenogeneic graft materials for improved release of P-15 peptides in a calvarium defect model. Journal of Craniofacial Surgery. 2014;25:70-6.
[8] Tovar N, Jimbo R, Witek L, Anchieta R, Yoo D, Manne L, et al. The physicochemical characterization and in vivo response of micro/nanoporous bioactive ceramic particulate bone graft materials. Materials Science and Engineering: C. 2014;43:472-80.

Effect of Drill Speed and Irrigation on Dental Implants

Ji Won Kang[1], Adam Alifarag[2], Chris Lopez[3], Nick Tovar[1], Lukasz Witek[1], Paulo Coelho[1]
[1]Department of Biomaterials and Biomimetics, New York University College of Dentistry, New York, NY, USA
[2]SUNY Upstate Medical University, Syracuse, NY, USA
[3]Icahn School of Medicine at Mount Sinai, New York, NY, USA

Introduction

Osseointegration is the direct contact between bone and implant without the interjection by non-bony tissue[1]. Early failure of osseointegration has been associated with implant design, surgical technique, or site infection[2]. As a key factor in implant survival rates, the primary, mechanical stability of the implant relies on the surgical technique implemented during the procedure[2-3]. Minimization of micromotion attributes to good primary stability of the implant which is crucial in the initial stages of osseointegration[4]. Micromotion greater than 150μm leads to resorption of bone and inhibition of growth of osteoblasts[5]. This hindrance of osteoconduction and bone remodeling necessitates the need for investigations in surgical methods for optimal primary stability. In this study, we investigate the effect of drilling speed and irrigation conditions on bone growth post implantation.

Methods

In twelve sheep (n=12), six screw root form endosseous titanium (Ti-6Al-4V alloy) implants (Bicon LLC, Boston, MA, USA) of 3.5mm or 6.0mm diameter were placed in each hip by varying drilling speeds (50, 500, and 1000 rpm) with and without irrigation. Implants (n=144), 36 in each size, 12 implants per drilling speed and 6 in each irrigation condition, remained *in vivo* for 3 or 6 weeks and subsequently extracted for histomorphometric analysis. Bone-implant contact (BIC) and bone area fraction occupancy (BAFO) were quantified using image analysis software (ImageJ, NIH, Bethesda, MD).

Results

BIC: There were no significant differences in BIC when comparing drilling speed within irrigation. The same trend applied for analysis within the non-irrigation group. However, implants placed by 50 rpm with irrigation had significantly higher BIC value than those placed with 50 and 500 rpm without irrigation.

BAFO: There was an increase from ~20% at t=3 weeks to ~35% at t=6 weeks and ~18% to ~26% for the 3.5mm and 6.0mm implant respectively. With the exception of implants placed by 50 rpm with no irrigation, no significant differences were found as an effect of irrigation conditions and drilling speeds.

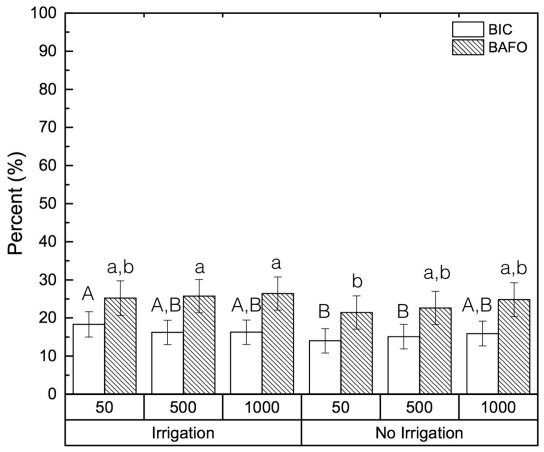

Figure 1: BIC and BAFO values (*f* (speed, irrigation)) showing difference in osseointegration and bone growth according to speed and irrigation condition

Conclusion

Results show that irrigation does not affect implant primary stability. Despite the positive correlation between bone volume and drilling speed, drilling speed is not an exclusive factor in successful osseointegration.

References

1. Mavrogenis, A. F., et al. Biology of implant osseointegration. *J Musculoskelet Neuronal Interact* 2009; 9(2): 61-71.
2. Giro, G., et al. The effect of simplifying dental implant drilling sequence on osseointegration: an experimental study in dogs. *Int J Biomater* 2013: 230310.
3. Blanco J, Alvarez E, Muñoz F, Liñares A, Cantalapiedra A. Influence on early osseointergration of dental implants installed with two different drilling protocols: a histomorphometric study in rabbit. *Clin. Oral Impl. Res.* 2011; 22, 92-99.
4. Sarendranath, A., et al. Effect of low speed drilling on osseointegration using simplified drilling procedures. *Br J Oral Maxillofac Surg* 2015;53(6): 550-556.
5. Gao SS, Zhang YR, Zhu ZL, Yu HY. Micromotions and combined damages at the dental implant/bone interface. *International Journal of Oral Science*. 2012;4(4):182-188.

Title: Fabrication and characterization of injectable sulfated carboxymethylcellulose hydrogels for nucleus pulposus replacement

Authors: Huizi A. Lin and Steven B. Nicoll
Institutions: The Department of Biomedical Engineering, The City College of New York, New York City, NY

Introduction: The development of an injectable nucleus pulposus (NP) replacement with structural and mechanical resemblance to the native tissue would serve as a promising minimally invasive treatment for early intervertebral disc degeneration [1,2,3]. Carboxymethylcellulose (CMC) is a low-cost, biocompatible anionic polysaccharide that has been shown to support mesenchymal stem cell chondrogenesis [4,5], and is a potential candidate material for NP repair. However, CMC lacks the negatively charged sulfate groups found on native glycosaminoglycans (GAG), which are important for tissue function. Moreover, GAG sulfation is essential for normal cartilage development and may enhance regenerative therapies [6,7]. Therefore, the objective of this study was to engineer sulfated CMC hydrogels and investigate the effects of macromer concentration and sulfate composition on hydrogel properties.

Materials and Methods: Methacrylated CMC (2%, 3%, and 4% (w/v)) was prepared as previously described [4,5], and the redox initiators, ammonium persulfate (APS) and tetramethylethylenediamine (TEMED), both at 10 mM, were added for radical polymerization [8]. Sulfation was achieved by the addition of 2-sulfoethylmethacrylate (2SEM) (0 mM, 1 mM, 5 mM, and 10 mM) to the reaction mixture. Sulfation was evaluated using the DMMB assay [4,5], and the equilibrium Young's modulus (E_Y) and the swelling ratio (Q_W) were measured as previously [4,5]. To assess cytotoxicity, human dermal fibroblasts were encapsulated at 4 x 10^6 cells/mL and the PicoGreen assay was used to determine DNA content [4,5]. A 2-way ANOVA with Tukey's post-hoc test was used to determine the effects of macromer concentration and 2SEM concentration on hydrogel properties (n=5; $p<0.05$; mean±SD).

Results: For all macromer concentrations, DMMB staining intensity increased and the amount of GAG equivalent significantly increased with higher 2SEM concentration (Fig. 1). No significant differences were detected across macromer concentrations. Q_W significantly decreased while E_Y significantly increased with higher macromer concentration (Fig. 2). The concentration of 2SEM did not have significant effects on hydrogel mechanical properties. No significant differences were observed for cytotoxicity of hydrogels from all groups (Fig. 3).

Discussion: This is the first study to investigate an injectable, sulfated CMC hydrogel system as a potential material for NP replacement. Although previous studies have demonstrated the use of CMC hydrogels for NP tissue engineering, sulfated CMC hydrogels were fabricated in the present work to better mimic both the structural and mechanical properties of the native tissue [4,5]. Sulfation of CMC hydrogels was confirmed and likely increased the fixed charge density based on the binding of cationic DMMB dye, but the degree of sulfation had no effect on functional properties (i.e., Q_W and E_Y). While the mechanical properties of all groups were within the range for native NP, 3% (w/v) gels were most similar and thus should be further explored [9].

Conclusion: Injectable sulfated CMC hydrogels were successfully fabricated and may serve as injectable, functional NP replacements.

Acknowledgements: The NSF for funding and Devika Varma at the City College of New York for technical assistance.

Figure 1. Qualitative DMMB staining and quantitative DMMB assay of sulfated-CMC hydrogels.

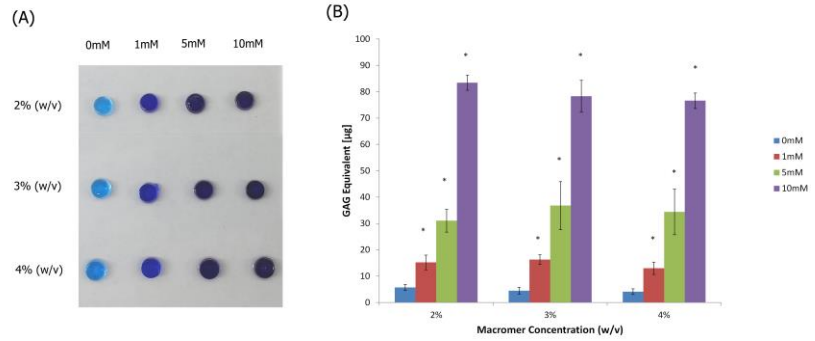

Figure 2. Swelling ratio and equilibrium modulus of sulfated-CMC hydrogels.

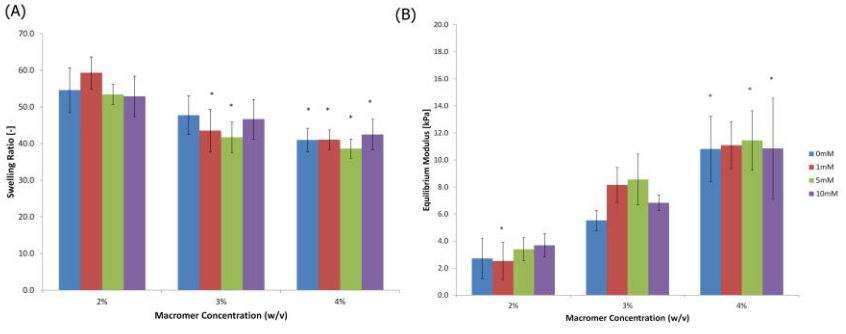

Figure 3. Cytocompatibility of sulfated-CMC hydrogels.

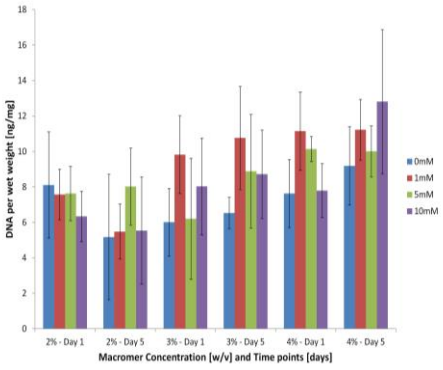

References:
[1] Francisco AT, et al (2013) Biomaterials 34:7381-8. [2] Smith LJ, et al (2014) Tissue Eng Part A 20:1841-9. [3] Sivan SS, et al (2014) Acta Biomater 10:1124-33. [4] Gupta MS, et al (2011) Tissue Eng Part A 17:2903-10. [5] Lin HA, et al (2015) J Biomed Mater Res A doi: 10.1002/jbm.a.25552. [6] Dawson PA (2011) Semin Cell Dev Biol 22:653-9. [7] Frith JE, et al (2013) Biomaterials 34:9430-40. [8] Varma DM, et al (2014) ORS Annual Meeting. [9] Cloyd JM, et al (2007) Eur Spine J 16:1892-8.

Modulation of Hydrogel Crosslinking Density to Promote Development of Functional Mechanical Properties in Engineered Cartilage

Eben G. Estell(1), MS, Andrea Tan, PhD(1), Sonia Bansal(1), Gerard Ateshian, PhD(1), Clark T. Hung, PhD(1).

1. Department of Biomedical Engineering, Columbia University, New York, NY, USA.

Introduction: Agarose hydrogels provide a reliable scaffold material for cartilage tissue engineering (1,2). Our laboratory has extensively employed a 2% (w/v) agarose scaffold to develop engineered cartilage with native equilibrium Young's modulus (EY) and proteoglycan (PG) content, but lacking native levels of collagen and dynamic modulus (G*), a measure of the functional tissue mechanical properties under physiologic loading (4). Previous studies have successfully increased collagen content by suppressing PG accumulation with chondroitinase-ABC but with no increase in G*(3), with recent efforts yielding a 20% increase above controls (5). This study investigates the modulation of scaffold density as an alternate strategy to control PG accumulation and thereby the biochemical makeup and mechanical properties of the tissue. Hydrogel concentration affects crosslinking density, pore size, and therefore hydraulic permeability and solute diffusivity. Higher density crosslinking associated with 3% agarose results in rapid elaboration of ECM that quickly plateaus as cells become starved of nutrients (6). Agarose scaffold density has been previously shown to influence PG release from the tissue and improve homogeneity by allowing diffusion throughout the tissue, which has been implicated in improving mechanical properties at equilibrium (7). We hypothesize that for juvenile (bovine) chondrocytes, low-density 1% agarose will leave more space for collagen elaboration by allowing PGs to be lost naturally via diffusion and, and thus yield tissues with superior mechanical properties under dynamic loading in comparison to the higher agarose concentrations previously employed. We additionally explore the use of this strategy with adult (human) chondrocytes.

Methods: Study 1. Chondrocytes were harvested and enzymatically digested from juvenile bovine knee joints, then expanded for one passage in DMEM containing 10% FBS, 1% PSAM, 5 ng/ml bFGF, and 5 ng/ml TGFβ1 (8). Chondrocytes were then seeded at 30M cells/mL in 1%, 2% and 3% agarose type VII (Sigma) and punched into constructs of 4mm diameter and 2.34mm thickness. All groups were cultured in serum-free DMEM containing 100 µg/ml Sodium Pyruvate, 50 µg/ml LProline, 1% ITS+, and 1% PSAM. Fresh media was changed on a 2-2-3 day schedule, supplemented with 50 µg/ml ascorbic acid and 100 nM Dexamethasone, and aliquots were saved for later analysis of PG content. All groups were supplemented with TGFβ3 for the first 14 days of culture (9). At day 0, 14, 28, 42, and 56 samples from each group (n=68) were mechanically tested under 10% strain in unconfined compression stress relaxation to extract EY, followed by dynamic compression (+/2% strain at 0.01Hz) to extract G*. Biochemical analysis was conducted to determine the GAG (indicative of PG content), hydroxyproline (indicative of collagen). Factorial ANOVA with Tukey post-hoc analysis was performed to evaluate the significance with $\alpha<0.05$. Study 2. Human chondrocytes were isolated from cartilage shavings obtained from clinical-grade allografts (14-year-old female) and prepared similarly as for bovine cells to yield 2% and 3% agarose constructs and analyzed for EY and G* at days 0, 14 and 28.

Results: Study 1. Over 56 days of culture 1% agarose yielded more compact constructs with significantly lower wet and dry weights. Compared to the GAG in the construct, GAG released into the media was highest in the 1% gel and during the first two weeks of culture, though never exceeding 35% of total GAG. Perhaps due to these relatively low release levels, no significant differences were observed in entrapped GAG content between the groups for the first 28 days, after which GAG in the 3% constructs plateaued. When normalized by wet weight at day 56 GAG levels in the 1% and 2% groups were similar and significantly higher than the 3% group (Fig. 1a). Collagen content in the constructs developed similarly and when normalized by wet weight at day 56 the 1% and 2% gels were similar and had significantly more collagen than the 3% group (Fig. 1b). Both EY and G* developed in similar manners, with the 1% and 2% groups increasing exponentially to day 56 while the 3% group followed a linear trend to significantly lower values. Both moduli increased with increasing gel concentration for the first 14 days and differences at even day 0 indicate that this initial trend is the result of differences in the agarose scaffold itself, while later differences arose as a result of the elaborated ECM. While the 2% gel achieved a significantly higher EY by day 42, the 1% gel continued to develop and was statistically similar to the 2% gel at day 56 (Fig. 2a). Both groups achieved nativelike EY around 700kPa and were significantly higher than the 3% group. The development of G* in the 1% gel surpassed the 3% agarose at day 42 and was significantly higher than both 2% and 3% gels by day 56 (Fig. 2b), yielding a 36% increase over the control. Study 2. When comparing the development of mechanical properties in this juvenile model with an adult human model, it

is evident that modulation of scaffold density must be tuned with the differing needs of these cells in mind. Contrary to the results in this study, 3% agarose yielded significantly higher EY in the adult human model (Fig. 3a&c), while G* behaved similarly to the juvenile model but did not significantly favor 2% agarose by day 28 (Fig. 3b&d).

Discussion: As anticipated, reducing the concentration of agarose to 1% from control values resulted in increased GAG release (Study 1). It appears that this enhanced the development of functional mechanical properties, where a significant 36% increase in G* was observed with 1% gels while maintaining nativelike EY. While 3% constructs had initially higher moduli, with culture time properties plateaued and yielded the lowest final properties of the group, confirming previous observations(6). Unexpectedly, while use of a lower density hydrogel increased the G* and maintained native PG levels and EY, as we have previously seen with chondroitinase-ABC treatment, there was no corresponding increase in collagen content over the control. The 1% gels were consistently smaller and lower in both wet weight and dry weight, indicating that this lower density gel may lead to the development of more compact tissues with altered swelling properties that may influence the quality and organization of the solid ECM rather than its biochemical content. The findings of Study 1 suggest that the structural interactions between GAG and collagen during tissue development in the 1% gel provide superior mechanical properties with less absolute ECM content for the bovine model. Further research is underway to better characterize the organization of the extracellular matrix, especially the collagen network architecture, and the interaction between collagen and PGs in the developing tissue. The disparate findings with juvenile (bovine, Study 1) and adult (human, Study 2) chondrocytes further suggests that scaffold crosslinking density may need to be tailored to the intrinsic biosynthetic capacity of the cell type adopted.

Significance: This study furthers efforts in cartilage tissue engineering to achieve native extracellular matrix composition and thus mechanical properties, thereby increasing the functionality and viability of engineered cartilage in vivo.

References: : 1. Buschmann, M. D. et al. J. Orthop. Res. (1992) 2. Mauck, R. L. et al. Methods (2000) 3. Bian, L. et al. Tissue Eng. Part A (2009) 4. Park, S. et al. Osteoarthritis Cartilage (2004) 5. O'Connell, G. D. et al. Eur. Cell. Mater (2014) 6. Ng, K. W. et al. J. Orthop (2005) 7. Kock, L. M. et al. Tissue Eng. Part A (2013) 8. Ng, K. W. et al. Tissue Eng. Part A (2009) 9. Lima, E. G. et al. Osteoarthritis Cartilage (2007)

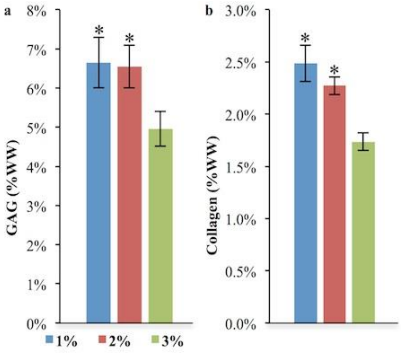

Figure 1: GAG (a) and collagen (b) content at day 56 normalized by construct wet weight. * $\alpha<0.05$ versus 3%.

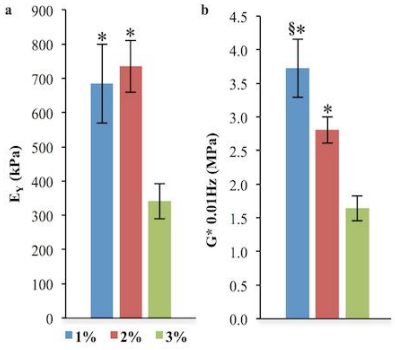

Figure 2: Equilibrium (a) and dynamic (b) moduli at day 56. * $\alpha<0.05$ versus 3%, § $\alpha<0.05$ versus 2%.

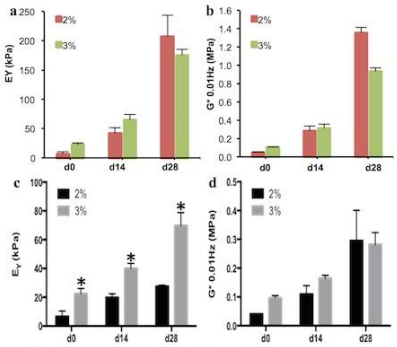

Figure 3: Equilibrium and dynamic moduli for juvenile bovine (a,b) and adult human (c,d) chondrocytes over early culture time. * $\alpha<0.05$ versus 2%.

Title: Characterization of a Model System to Study Synovial Membrane Transport Properties

Authors: Robert Stefani, BS, Andrea R. Tan, PhD, Adam B. Nover, MS, J Chloe Bulinski, PhD, Gerard Ateshian, PhD, Clark Hung, PhD.

Institutions: Columbia University, New York, NY, USA.

Introduction: The native synovium is mainly composed of macrophages and fibroblast-like synoviocytes contained in a dense extracellular matrix. The synovium lines the articular surfaces of the joints, secreting lubricating and inflammatory molecules into the joint space. In order to fully understand the interplay of cytokines and other molecules in the synovial fluid in contact with cartilage, we must also understand the semi-permeable nature of the synovium. Studies have evaluated the transport of large lubricant molecules such as HA and lubricin across a model synovial monolayer, however the movement of smaller inflammatory cytokines has been ignored [2]. As such, the aim of this study aimed to characterize the transport properties of synovial cell monolayers on a transwell filter system, a system that has been well established for making such impedance measurements of epithelial and endothelial cell monolayers.

Methods: Juvenile bovine synovial tissue was harvested and digested in collagenase type IV. After filtration, synovial cells were expanded in alpha-minimum essential medium containing 10% FBS, antibiotics, and 5 ng/ml FGF-2 at a seeding density of 1760 cells/cm2. To create an in vitro synovial layer, passage 2 synovial cells were seeded at 100,000 cells/cm^2 on 12 mm transwells (3 μm, polyester membrane). Sheets were grown for four days in growth medium consisting of DMEM with 10% FBS and 50 ug/ml ascorbic acid-2-phosphate, which has been shown to support the growth of a membrane layer [1]. Following two days of serum starvation (DMEM with 0.5% FBS), sheets were treated with 10 ng/ml IL-1α for three days. After IL-1 treatment, growth media was reintroduced for a three day recovery period.

Cell sheet integrity and solute permeability were assessed throughout the study. An Endohm 12 chamber was used to measure the transmembrane resistance values both pre- and post- IL-1 treatment and after the recovery phase. Transmembrane resistance (commonly referred to as TEER) is a common measure of endothelial monolayer integrity. To model the passive diffusion characteristics of a small molecule, 10 kDa FITC-labeled dextran was added to the top chamber of the transwell and samples were collected from the bottom well at 1, 4, 8 and 24 hour time points. Dextran was quantified by measuring fluorescence signal on a plate reader (485/535 nm). 10 kDa dextran was chosen as a molecule of comparable size to inflammatory cytokines in the joint, such as IL-1 and TNF-α and 70 kDa dextran was used to model the approximate size of TGF-β. The general morphology and viability of the cell sheets was assessed using a LIVE/DEAD calcein/ethidium bromide stain. Immunohistochemistry was conducted by fixing transwells in 4% paraformaldehyde and staining for lubricin (rabbit polyclonal primary antibody, FITC-conjugated goat anti-rabbit secondary antibody). Statistics were performed using a paired student's t-test and error bars show the standard error.

Results: The engineered synovium exhibited characteristics of native synovium, and had the expected solute transport properties (Figure 1). Live/dead staining of a synovial cell sheet grown on a transwell filter showed high viability and morphology similar to native synovium. Immunohistochemistry staining of lubricin showed moderate staining in the control group and intense staining in IL-1 treatment group. Flux of 10 kDa dextran was significantly greater than the flux of 70 kDa dextran after 24 hours. In the interleukin-treatment study, flux across interleukin-treated cell sheets was significantly greater than the flux across control cell sheets at one hour (Figure 2). After one hour, approximately 16% and 20% of the total dextran had diffused through the control and IL-1 treated sheets, respectively. Transmembrane resistance normalized to pre-treatment values showed that the control group significantly decreased post-treatment and IL-1 did not.

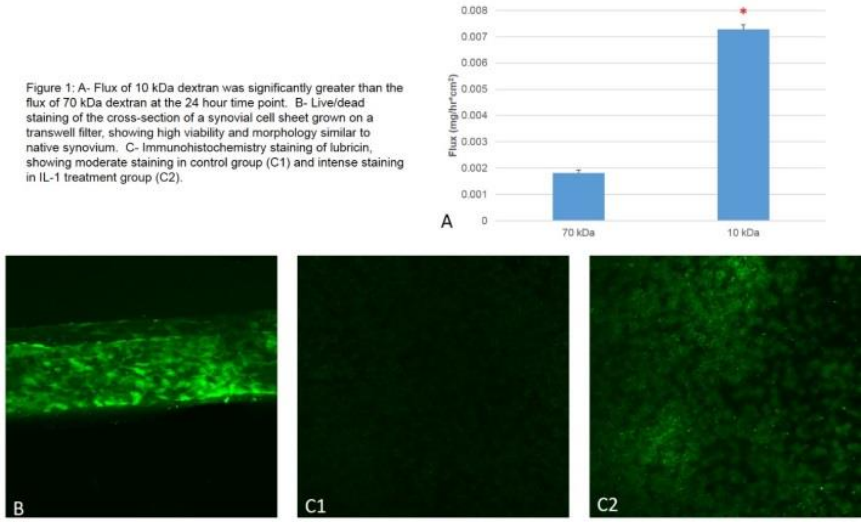

Figure 1: A- Flux of 10 kDa dextran was significantly greater than the flux of 70 kDa dextran at the 24 hour time point. B- Live/dead staining of the cross-section of a synovial cell sheet grown on a transwell filter, showing high viability and morphology similar to native synovium. C- Immunohistochemistry staining of lubricin, showing moderate staining in control group (C1) and intense staining in IL-1 treatment group (C2).

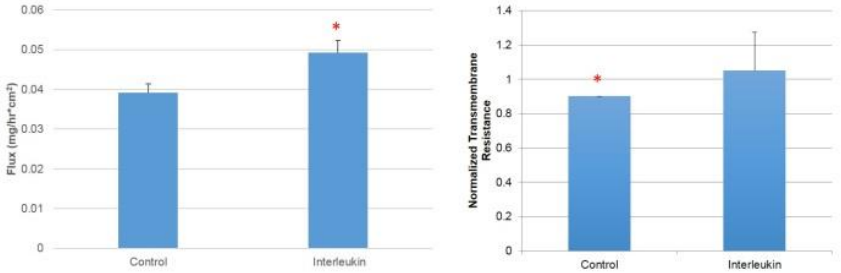

Figure 2: Left- At one hour time point, flux of interleukin-treated cell sheets was significantly greater than the flux of control cell sheets. Right- Transmembrane resistance normalized to pre-treatment values showed that control group significantly decreased post-treatment and IL-1 did not.

Discussion: We have described a tissue engineered cell sheet that is similar in morphology and lubricin content to native synovium. The transport of small (and large) molecules across this sheet can be readily quantified using established techniques, and we have identified temporal differences due to inflammatory cytokines. In the current study, we established our ability to grow a multilayered synovial cell membrane atop a transwell filter. Measures of solute transport across this synovial membrane demonstrated anticipated increases in solute diffusivity with decreasing solute molecular weight. The synovial membranes were able to respond with increased production of lubricin when exposed to interleukin, in support of findings by Blewis, et al. who showed increased lubricin release into the media of groups treated by IL-1 [2]. Additionally, measures of transmembrane resistance showed modulation of baseline impedance. These studies will help to establish a model system that can contribute fundamental information regarding the transport across synovial membranes, providing a tool for research as well as development of tissue engineering strategies for engineering the synovium [3].

Significance: These studies will help to establish a model system that can contribute fundamental information regarding the transport across synovial membranes, providing a tool for research as well as development of tissue engineering strategies for engineering the synovium [3].

References: 1-Yu, et al. Biomaterials 35 (2014) 3516-3524. 2- Blewis, et al. Bioeng Biotech 106 (2010) 149-160. 3- Erdogan, et al. Mater Res Part A 2014.

Investigating Actuating Poly(Ethylene Glycol) Based Hydrogels for Tissue Engineering

Daniel P. Browe (1); Tracy Scott (1); Joseph W. Freeman (1)

1. Department of Biomedical Engineering; Rutgers, The State University of New Jersey; Piscataway, NJ, USA

Introduction: Many researchers use growth factors to enhance tissue development on implantable scaffolds. Although growth factors are important for natural tissue development cells are also subjected to other types of stimulation including mechanical strain and electrical stimulation. In order to exploit these responses for regenerative purposes we are developing a series of electroactive polymers that respond to electrical stimulation by changing in size or shape[1], These polymers have charged side-chains and form ionic electroactive hydrogels (IEHs) when crosslinked. They bend in an electric field due to ion movement which causes reversible, asymmetric swelling[1,2]. In this study we present an anionic and cationic IEH based on poly (ethylene glycol) (PEG) and investigated the role of side chain chemistry on IEH movement and biocompatibility.

Materials and Methods: The hydrogels produced and tested in this study were formed from Acrylic Acid (AA) monomer and 2-(Methacryloyloxy)ethyl]trimethylammonium chloride (MAETAC) monomer (Sigma-Aldrich) and PEG diacrylate (MPD Chemicals Company). A photo-initiator solution of 2,2-Dimethoxy-2-phenylacetophenone in 1-vinyl-2-pyrrolidinone (300 mg/mL, Sigma-Aldrich) was used to facilitate cross-linking of the hydrogel while under UV radiation for 1-2 minutes. Hydrogel sheets were crosslinked with various ratios of PEG to AA or MAETAC (g/g). To test the amount of actuation, the samples were placed in PBS equi-distant between two Platinum electrodes. Electric stimulation in the form of 20 V of DC Voltage was applied for 1 minute, followed by another 1 minute with the electric field reversed in direction. The movement of the samples was captured via camera and analyzed via ImageJ. A basic test of biocompatibility was performed by seeding C2C12 mouse myoblasts on hydrogel samples and measuring proliferation with a Presto Blue Assay ®. Statistics were performed using an ANOVA and a Tukey's post-hoc test ($p < 0.05$).

Results and Discussion: The amount of angular movement in degrees was measured for all samples, shown in figure 1A for PEG-AA. The amount of movement in the hydrogel seemed to increase with an increase in the amount of monomer. In PEG-AA hydrogels after the ratio reached 1:8, the movement plateaued, PEG-MAETAC displayed a downward trend with increasing MAETAC. Biocompatibility tests show that a 1:4 ratio of PEG to AA was best for C2C12 attachment and proliferation, figure 1B. A 1:0.6 ratio of PEG to MAETAC was best for C1C12 proliferation. Groups with higher concentrations of AA and MAETAC produced environments that were too acidic or basic for optimal cell proliferation.

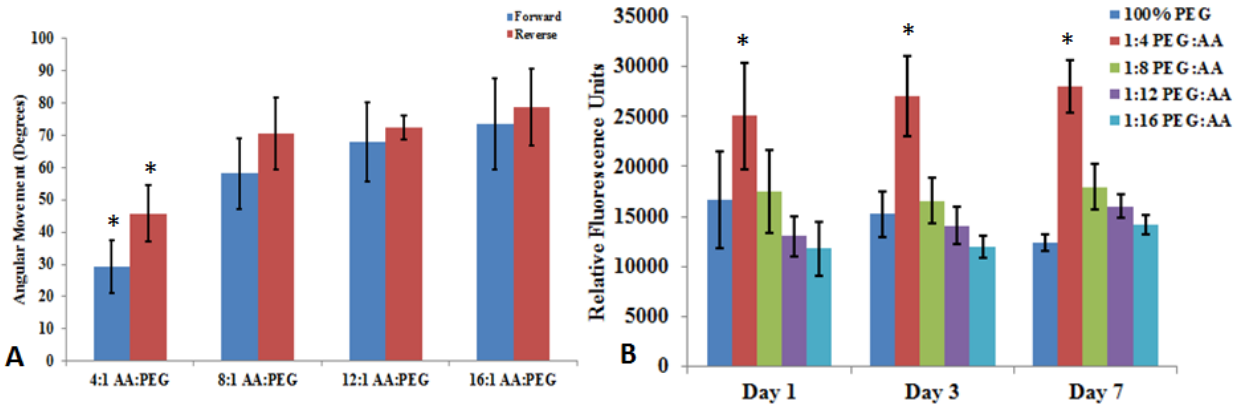

Figure 1. (A) Angular movement in degrees for hydrogels with different ratios of AA to PEG **(B)** Metabolic activity on hydrogels with different ratios of AA to PEG (* indicates statistically significant, $p < 0.05$).

Conclusions: PEG-AA and PEG-MAETAC IEHs were formed and tested for their biocompatibility and ability to actuate in an electric field. The amount of angular movement was proportional to the amount of AA but not MAETAC We determined that myoblasts will attach and grow on these hydrogels with the optimal ratio being close to 1:4 PEG:AA and 1:0.6 PEG:MAETAC. Future experiments will test changes in cell differentiation and fusion occurring on these hydrogels during actuation.

Acknowledgements: We are grateful for funding from the following: NSF grant ECCS 1408202; The NIH under Ruth L. Kirschstein National Research Service Award T32 GM8339 from the NIGMS; and Myos Corporation.

References: [1] Bar-Cohen, Y. 2004. SPIE—The International Society for Optical Engineering. ISBN: 0-8194-5297-1. [2] Shahinpoor, M; Kim, KJ. Smart Mater. Struct. 2001. 10: 819-833.

Evaluating a biodegradable piezoelectric composite scaffold for cartilage tissue engineering applications.

Ateka Khader and Treena Livingston Arinzeh
Biomedical Engineering, New Jersey Institute of Technology, Newark, NJ, USA

Introduction: Cartilage and bone tissue have known piezoelectric properties, which means they can generate electrical activity in response to mechanical deformation. Using a biomimetic approach, Zinc oxide (ZnO), which has known piezoelectric properties, was fabricated into a flexible 3-D fibrous scaffold by embedding ZnO nanoparticles into a slow degrading polycaprolactone (PCL) fiber. Zinc ions can be released from the fiber over time which also may be beneficial for cell function since zinc has well known insulin mimetic properties. Insulin and insulin growth factors play important role in chondrogenesis and cartilage formation. In this study, ZnO-PCL composite fibrous scaffolds were evaluated for the first time for MSCs chondrogenesis, examining MSC growth and differentiation by matrix production.

Materials and Methods: 1, 2.5, 5 and 10 wt% of ZnO nanoparticles (100nm) to PCL were dissolved in methylene chloride. Nonwoven fibrous ZnO-PCL composite scaffolds were fabricated using electrospinning. Scanning electron microscopy (SEM) and Image J software were used to determine the fiber morphology and the average fiber diameter. 10mm samples were incubated in PBS and the release of zinc were determined by using inductive coupled plasma mass spectrometry (ICP-MS) over time. Human MSCs were seeded onto the scaffolds at $1.76*10^5$ cells/cm^2 and cultured for 28 days in chondrogenic induction media. Samples were harvested and analyzed at days 14 and 28. Cell number (n=4 per group) was determined using PicoGreen® ds DNA assay (Invitrogen). Immunostaining for collagen type II and cell morphology using actin staining were evaluated by confocal microscopy.

Results and Discussion: SEM images showed comparable fiber morphology, fiber diameters and interfiber spacing in the micron-range of different ZnO composite scaffolds (figure 1). Zinc release was higher for higher concentrations of ZnO in the composite scaffolds after day 1 and 7 (figure 2) which could contribute to MSCs chondrogenesis. There was a significant increase in cell number in ZnO composite groups as compared with PCL alone at day 14 (figure 3). Cells also appeared to produce more collagen type II in ZnO composite groups as compared to control (Figure 4).

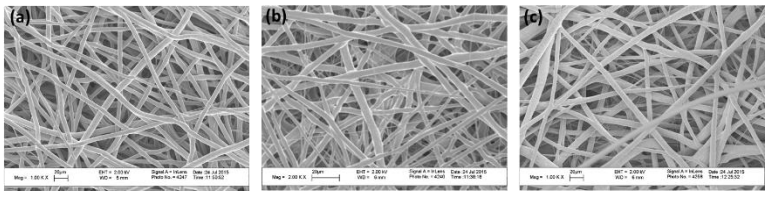

Figure 1: SEM images showing fiber morphology of (a) PCL, (b) 1%ZnO and (c) 10%ZnO. Scale bar = 20 um.

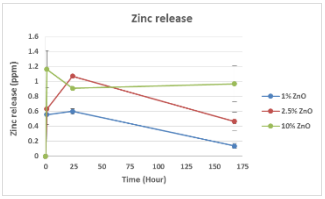

Figure 2: Zinc release from the scaffolds.

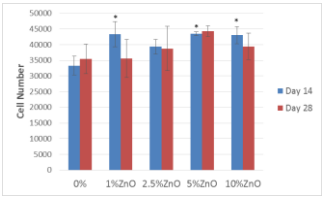

Figure 3: Cell number at day 14 and 28 on ZnO-PCL scaffolds.*P<0.05

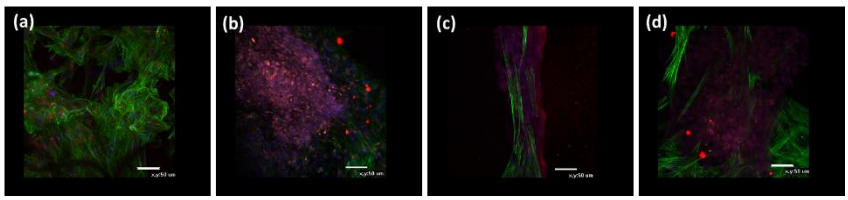

Figure 4: Confocal images showing collagen type II (red), Actin (green) and nucleus (blue) on (a) PCL control, (b) 1%ZnO (c) 5% ZnO and (d)10%ZnO composite. Scale bar= 50µm

Conclusion: ZnO composite scaffolds support cell growth and attachment. ZnO composite can promote chondrogenic differentiation of MSCs as observed by an increase in collagen type 2 production. This study demonstrated the feasibility of ZnO as a potential scaffold for cartilage tissue engineering. Future studies will apply mechanical loading to the scaffolds to investigate the effect of piezoelectric activity on the MSC chondrogenesis.